ISTANBUL TECHNICAL UNIVERSITY ★ GRADUATE SCHOOL

MODELLING AND SIMULATION OF THE PEM FUEL CELL ON MQ1-PREDATOR UNMANNED AIR VEHICLE

M.Sc. THESIS

OSMAN SÖZEN

Energy Science And Technology Division

Energy Science and Technology Programme

AUGUST 2024

ISTANBUL TECHNICAL UNIVERSITY ★ GRADUATE SCHOOL

MODELLING AND SIMULATION OF THE PEM FUEL CELL ON MQ1-PREDATOR UNMANNED AIR VEHICLE

M.Sc. THESIS

OSMAN SÖZEN
(301201058)

Energy Science And Technology Division

Energy Science and Technology Programme

Thesis Advisor: Prof. Dr. İlhan KOCAARSLAN

AUGUST 2024

İSTANBUL TEKNİK ÜNİVERSİTESİ ★ LİSANSÜSTÜ EĞİTİM ENSTİTÜSÜ

MQ-1 PREDATOR İNSANSIZ HAVA ARACINDA PEM TİPİ YAKIT PİLİNİN MODELLEME VE SİMÜLASYONU

YÜKSEK LİSANS TEZİ

OSMAN SÖZEN
(301201058)

Enerji Bilim ve Teknoloji Anabilim Dalı

Enerji Bilim ve Teknoloji Programı

Tez Danışmanı: Prof. Dr. İlhan KOCAARSLAN

AĞUSTOS 2024

Osman SÖZEN, a M.Sc. student of ITU Institute of /Graduate School of Science Engineering student ID 301201058, successfully defended the thesis entitled ‘’MODELLING AND SIMULATION OF THE PEM FUEL CELL ON MQ-1 PREDATOR UNMANNED AIR VEHICLE’’ which he prepared in front of the jury, whose signatures are below, having complied with the conditions outlined in the relevant legislation.

Thesis Advisor :	**Prof. Dr. İlhan KOCAARSLAN** Istanbul Technical University	.....
Jury Members :	**Assoc. Prof. Dr. İlker ÜSTOĞLU** Istanbul Technical University	.....
	Assoc. Prof. Dr. Emre ÖZER Istanbul University	.....

Date of Submission : 24.07.2024
Date of Defence : 07.08.2024

To my precious family,

FOREWORD

I want to dedicate this research to my family, my wife and my big brother in particular, who have provided me with unwavering spiritual support throughout this time.

August 2024

Osman SÖZEN
(Mechanical Enginer)

CONTENT

Page

ABBREVIATIONS

AFC **:** Alkaline Fuel Cell
APU **:** Auxiliary Power Units
BR&TE **:** Boeing Research & Technology Europe
CO **:** Carbon Monoxide
CO2 **:** Carbon Dioxide
CH4 **:** Methane
DC **:** Direct Current
DMFC **:** Direct Methanol Fuel Cell
GHG **:** Greenouse Gas
GDL **:** Gas Diffusion Layer
HALE **:**High Altitude Long Endurance
HHV **:** Higher Heating Value
H2 **:** Hydrogen
H2O **:** Hydrogen Dioxide
LHV **:** Lower Heating Value
MEA **:** Membrane Electrode Assembly
OER **:** Oxygen Excess Ratio
PTFE **:** Polytetrafluoroethylene
SOFC **:** Solid Oxide Fuel Cell
SO2 **:** Sulphure Dioxide
PAFC **:** Phosphoric Acid Fuel Cell
PEM **:**Proton Exchange Membrane
PEMFC **:**Proton Exchange Membrane Fuel Cell
UAV **:**Unmanned Aerial Vehicle

SYMBOLS

P_{atm}	:Atmospheric pressure, atm
T_{atm}	:Atmospheric temperature, °C
W_{cp}	:Compressor speed, rad/sn
J_{cp}	:Combined inertia for the motor, kg.m^2
τ_{cm}	:Torque input to the compressor motor, N.m
τ_{cp}	:Torque need by the compressor, N.m
η_{cm}	:Mechanical efficiency of the motor, %
W_{cl}	:Mass flow rate of the cooler, kg/s
$W_{v,cl}$	:Mass flow rate of the vapor, kg/s
$W_{a,cl}$	:Mass flow rate of the dry air, kg/s
$P_{a,cl}$	:Dry air pressure, bar
$P_{v,cl}$	:Vapor saturation pressure, bar
P_v	:Pressure of the water vapor in the mixture, bar
P_{sat}	:Saturation pressure of the vapor at the temperature of the mixture, bar
Φ	:Ratio of humidity
M_a	:Molar mass of dry air, kg/mol
M_v	:Molar mass of vapor, kg/mol
Ω	:Humidity ratio, %
$W_{v,hm}$	:Mass flow rate of the vapor at humidifer outlet, kg/s
$W_{v,cl}$	:Mass flow rate of the cooler at humidifer outlet, kg/s
$W_{v,inj}$	:Mass flow rate of the water injected, kg/s
W_{hm}	:Mass flow rate at the humidifier, kg/s
$\dot{m}$	:Mass flow rate, kg/s
Cp_{water}	:Heat capacity of water, J/ kg. K
U	:Overall heat transfer coefficient, W/m^2.K
A	:Heat transfer area of the radiator, m^2
p	:Density of water, kg/m^3
ΔT_{lm}	:Log-mean temperature, Kelvin
V_{fan}	:Voltage of the fan, Volt
V_{pump}	:Voltage of the pump, Volt
D_{nt}	:Nozzle throat diameter, m^2
η	:Isentropic coefficient
R_g	:Gaz constant, J/K-mol
κ	:Specific heat ratio of the gas in the primary flow
N_{cell}	:Cell number of the stack
M_{H2}	:Molar weight of hydrogen, gr/mol
F	:Faraday's constant
V_{cell}	:Cell Voltage, Volt
E_{Nerst}	:Nerst Potentail Energy, Volt
V_{act}	:Activation Losses, Volt
V_{ohm}	:Ohmic Losses, Volt
V_{con}	:Concentration Losses, Volt
$W_{H2,reacted}$	:The amount of hydrogen consumed in the reaction, kg/s
N	:Number of cells in the stack
I	: Current, Amper
M_{H20}	:Molecular weight, kg/mol
P_i	:Pressure of component, bar
m_i	:Mass, kg

$\mathbf{V}$	:Volume, m^3
$\mathbf{k_{ca,out}}$	:Orifice constant
$\mathbf{T_{stack}}$	:Stack temperature, ºC
$\mathbf{T_{membrane}}$	:Membrane thickness, mm
$\mathbf{T_{GDL,A}}$	:Anode GDL thickness, mm
$\mathbf{T_{GDL,C}}$	:Cathode GDL thickness, mm
$\mathbf{I_o}$	:Exchange current density, A/cm^2
$\mathbf{I_L}$	:Limiting current density, A/cm^2
alpha	:Charge transfer coefficient
$\mathbf{rho_{membrane}}$	:Density of dry membrane, kg/m^3
$\mathbf{W_{v,inj}}$	:Amount of water injected into the air flow, kg/s
$\mathbf{\Phi^{des}}$	:Desired stack inlet humidity (%)
$\boldsymbol{\upsilon_{fcv}}$	:Control input signal of the valve, 0 to 1
$\mathbf{W_{fcv,max}}$	:Maximum flow rate, kg/s
$\mathbf{y}$	:Mass fraction
$\mathbf{a_w}$	:Water activity
$\boldsymbol{\lambda_{O2}}$	:Oxygen exchange ratio (OER)

LIST OF TABLES

LIST OF FIGURES **Page**

MODELLING AND SIMULATION OF THE PEM FUEL CELL ON MQ-1 PREDATOR UNMANNED AIR VEHICLE

SUMMARY

In today's world, the Unmanned Aerial Vehicle (UAV) is becoming more and more important for both military and civilian purposes. Due to its size, which is similar to that of a general aviation aircraft, and its lengthy endurance (several days), it can operate without a human pilot for extended periods of time while carrying significant payloads and instrumentation.

However, at that time, electrical unmanned aerial vehicles (UAVs) were growing in popularity because they contributed to reducing carbon dioxide emissions and enabling more sustainable aviation. These UAVs are primarily powered by hydrocarbon fuels, and their design is heavily limited by the reciprocating engines used in general aviation, which are made for entirely different requirements. Considerable research has been done on the design implications that come from using electric propulsion in a wide range of unmanned air vehicles.

Due to threats like climate change and the disruption of natural equilibrium, decarbonized energy sources are becoming very popular and they are supported by government investments and incentives. This is done in an effort to lessen reliance on fossil fuels. Infrastructure-wise, renewable energy solutions are expensive. They have, meanwhile, been keeping up their technological advancement quite rapidly. With the help of new technical advancements, the goal is to make those systems more efficient and so reduce the initial investment expenses.

The primary determinant of a UAV performance in case the air vehicle is integrated with PEMFC system is energy which has huge effect on mission capability of the air vehicle. Proton exchange membrane (PEM) fuel cells are designated as the principal power source for electrified unmanned aerial vehicles (UAVs) because they have a significantly higher power density than other fuel cell types and a larger potential for use in high altitude long endurance (HALE) UAV flights.

The aviation industry is mostly to blame for the majority of the emission gasses from fossil fuels that are released into the atmosphere. Since fuel cell powered air vehicles frequently have PEM type fuel cells, only water vapor is released to the atmosphere of the MEA during electrochemical reaction. Using hydrogen as fuel over fossil fuels is considered as a substantial alternative in reducing detrimental emissions to the environment. Many studies are being conducted now with the purpose of developing fuel cell technology's longevity and efficiency for the aviation sector.

Since, PEMFC is very efficient, emits no emissions, and can function at low temperatures, it is a highly productive source of electricity for more and all-electric air

vehicles. Finding a direct experimental estimate of the PEM fuel cell's real performance using a variety of characteristics and operating conditions, such as chemical reactions, fuel pressure, working temperature, and humidity, is difficult, though. As a result, modeling is crucial to comprehending PEM fuel cell operational performance.

In order to achieve this meet, energy-related procedure for unmanned airvehicle which are designed with a specific fuel cell type was investigated in this work. First, UAV's mission profile and specifications were established. Based on mission objectives, the MQ-1 Predator was chosen as a reference, and some input characteristics were taken for granted.

This thesis could be helpful for ongoing and upcoming research. The models are generated based on relevant studies which have been conducted up to now. The study includes modelling for not only for membrane electrode assmebly but also humidifier, anode and cathode sides, hydrogen source and oxygen sources. Therefore, it can be truly interpreted that the models of each equipment integrated in PEM fuel cell stack will be great guidance for the other users who are being worked on.

MQ-1 PREDATOR İNSANSIZ HAVA ARACINDA PEM TİPİ YAKIT PİLİNİN MODELLEME VE SİMULASYONU

ÖZET

İnsansız Hava Aracı (İHA), günümüz dünyasında hem sivil hem de askeri uygulamalarda giderek artan bir öneme sahip olmaktadır. Genel havacılık uçaklarıyla karşılaştırılabilecek büyüklükte olması ve günlerce süren uzun uçuş ömrü, ağır yükleri ve enstrümantasyonu, bir pilota ihtiyaç duymadan uzun süre taşıyabilmesine olanak tanıyor.

Günümüzde, elektrikli insansız hava araçları, karbondioksit emisyonunun azaltılmasına yardımcı olmaları ve esas olarak hidrokarbon yakıtlarla çalışan daha sürdürülebilir havacılık sağlamaları ve tasarımının mevcut genel havacılık pistonlu motorları tarafından çok fazla kısıtlanması nedeniyle giderek daha popüler hale geliyorlar ve tamamen farklı gereksinimlere yönelik olarak tasarlanmışlardır. Elektrikli tahrik çözümlerinin küçük ve orta büyüklükteki İHA'lara ve aynı zamanda bu türdeki büyük İHA'lara dahil edilmesinden kaynaklanan tasarım etkileri etrafında önemli miktarda araştırma yapılmıştır.

İklim değişikliği ve ekolojik dengenin bozulması gibi riskler nedeniyle, fosil yakıtlara olan bağımlılığın azaltılması amacıyla hükümetlerin çeşitli teşvik ve yatırımlarıyla her geçen gün daha da popülerlerleşen hidrojen gibi temiz enerji kaynaklarına yönelim giderek artış göstermektedir. Yenilenebilir enerji sistemleri altyapı açısından pahalıdır. Ancak teknolojik gelişmelerini çok hızlı bir şekilde sürdürüyorlar. Bu sistemlerin verimliliğinin arttırılması amaçlanmakta ve böylece yeni teknolojik gelişmelerle birlikte ilk yatırım maliyetleri azalmaktadır.

Enerji, proton değişim membranlı yakıt hücresi (PEMFC) sistemine sahip küçük bir insansız hava aracının (İHA) performansını belirleyen en önemli faktördür çünkü küçük bir İHA'nın görev kapasitesi, güç kaynağının enerjisi tarafından belirlenir. Proton değişim membranlı (PEM) yakıt hücresi, diğer yakıt hücresi türleriyle karşılaştırıldığında çok yüksek güç yoğunluğuna ve dolayısıyla yüksek potansiyele sahip olduğundan, yakıt hücresiyle çalışan insansız hava araçları (İHA) için özellikle birincil güç kaynağı olarak kabul edilir. yüksek irtifa uzun havada kalma İHA uçuşlarında kullanılmaktadır.

Fosil yakıtlardan çevreye yayılan emisyon gazlarının önemli bir kısmı havacılık sektöründen kaynaklanmaktadır. Havacılık sektöründe, hidrojenle çalışan araçlarda sıklıkla hidrojen oksijenle birleşen Polimer Elektrolit Membran (PEM) yakıt hücreleri kullanıldığından, fosil yakıtlar yerine hidrojenin yakıt olarak kullanılması, doğaya zararlı emisyonların azaltılmasında önemli bir alternatif olarak değerlendirilmektedir. Elektrokimyasal reaksiyonlar sayesinde enerji üretilirken membran düzeneğinin dışına

yalnızca su buharı salınır. Günümüzde yakıt hücresi teknolojisinin havacılık endüstrisine yönelik verimliliğini ve dayanıklılığını arttırmayı amaçlayan çok sayıda çalışma bulunmaktadır.

Bir polimer elektrolit membranlı (PEM) yakıt hücresi, çok verimli olması, emisyon içermemesi ve düşük sıcaklıkta çalıştırılması nedeniyle daha fazla ve tamamen elektrikli hava aracı için elektrik üretimi açısından çok verimlidir. Ancak PEM yakıt hücresinin gerçek performansının kimyasal reaksiyonlar, yakıt basıncı, çalışma sıcaklığı ve nem gibi çeşitli parametreler ve çalışma koşulları aracılığıyla doğrudan deneysel tahminini bulmak o kadar kolay değildir. Bu nedenle modelleme, PEM yakıt hücresinin operasyonel performansını anlamada önemli bir rol oynar.

Bu nedenle bu talebi karşılamak amacıyla bu çalışma kapsamında PEMFC sistemli bir İHA enerji açısından incelenmiştir. İlk olarak bir İHA'nın görev profili ve gereksinimleri belirlendi. Referans olarak görev gereksinimlerine göre MQ-1 Predator seçilmiş ve bu referans uçaklara dayalı analizler yapabilmek için yakıt piline bağlı olarak bazı girdi parametreleri ve bazı ilgili kabuller yapılmıştır.

Çalışma, yakıt hücresi yığınının en önemli ekipmanı olan membran elektrot düzeneğinin yanı sıra nemlendirici, anot ve katot gaz kanalları, soğutma sistemi, hidrojen kaynağı ve oksijen kaynaklarına yönelik modellemeleri içermektedir. Bu nedenle, PEM yakıt hücresi yığınına entegre edilen her bir ekipmanın modelinin, üzerinde çalışılan diğer kullanıcılar için büyük bir yol gösterici olacağı ve kullanıcının, modeli mevcut bilgi ve verilere göre uyarlamasına olanak sağlayacağı doğru bir şekilde yorumlanabilir.

Ekipman ve yakıt pli yığın yapısının modellemesine ek olarak, sistemde hava aracının anlık güç ihtiyacını karşılamak için sisteme entegre edilen kontrol arayüzleri de mevcuttur. Oksijen kaynağı tarafında kompresör ekipmanında ve soğutma sistemi içerisinde kullanılan pompa ekipmanının debi kontrollerinde, hata oranını azaltmak için integral ve yerleşmeyi hızlandırmak için de oransal kontrol uygulanması gerektiğinden PI kontrol metodu uygulanmıştır.

Termodinamik hesaplamalar, hem anot hem de katot tarafında orantılı kontrol metodolojisinin tercih edildiğini göstermektedir, çünkü orantılı kontrolör geçici etkileri azaltabilir ve istenen neme ulaşmak için su enjeksiyonunun kontrolünü nispeten basit hale getirebilir. Bu yüzden nemlendirici kontrolünde hem anot hem de katot taraflarında oransal kontrol yöntemi uygulanmıştır.

Öte yandan bir diğer önemli kontrol uygulaması ise hidrojenin sisteme yeniden sirküle edilmesidir. Bu kontrol kısmında ise ileri beslemeli kontrol sistemleri giriş sinyalindeki değişikliklere daha hızlı yanıt verdiğinden, ileri beslemeli akım düzenlemesi ve hidrojen akış hızı kontrolü birleştirilmiştir.

Gerçek uygulamalarda uygulanması gereken bir diğer kontrol yöntemi ise, anot tarafındaki nitrogen atık kontrolüdür. Çünkü, nitrogenin konsantrasyon yüzdesi arttıkça hidrojenin konsantrasyonu düşeceğinden, nitrogenin bir bölümünün dış ortama atılması ve bunun kontrolünün yapılması gerekmektedir. Ancak bu çalışmada bu atık kontrolü sistemi çok karmaşık hale getirdiğinden uygulanmamıştır. Bir diğer gerçek uygulamalardan sapma ise kompresör tarafındadır. Bu çalışmada kompresörün verimi100% olarak kabul edilmesidir. Ancak, gerçek çalışma prensibinde kayıplar oluşacaktır ve hiçbir zaman kompresör kayıpsız veya 100% verimle çalışamamaktadır.

Havacılık uygulamalarında yaygın olarak gördüğümüz yöntem, yakıt pili ve bataryanın hibrit system şeklinde kullanılmasıdır. Hibrit çözüm ile birlikte, hava aracının kalkış veya tırmanış anındaki güç ihtiyacının yakıt pili tarafından karşılanamaması durumunda batarya devreye girer ve anlık güç ihtiyaçları batarya ile karşılanmış olur. Ancak, bu çalışmada tek bir yakıt pili tarafından güç ihtiyacının karşılanması hedeflenmiştir.

Bu çalışma, potansiyel olarak bu tür sistemlerin devam eden araştırmalarına ve çevredeki diğer çeşitli bileşenlerin modellenmesine katkıda bulunabilir. Modeller, bu konularla ilgili ilgili araştırmalara dayanarak oluşturulur.

1. INTRODUCTION

These days, the aviation industry makes a substantial contribution to the socioeconomic advancement of several nations worldwide. Over the past 20 years, air travel capacity has grown dramatically, and until 2030, it is predicted to grow by about 5% yearly [1]. Surely, this will end up with increasing the number of active aircrafts Based on Boeing market overview [2], Approximately 47,000 operational planes are expected by 2036, up from 23,000 in 2016. Although an aircraft's overall weight capacity determines how much weight it can carry, most commercial flights have rouhly 640 tm MTOW [3]. Large engines that use a lot of kerosene-based fuel are required for a plane to conduct their missions under these high level of MTOWs. Due to the enormous load, there is a significant need for aviation fuel, which raises concerns and has implications for efficiency, cost, safety, and specific energy. The majority of fuels used in aviation today are petroleum-based compounds derived from fossil fuels. [3,4]. Kerosene is the fuel that is utilized in the aviation sector the most frequently among all other fuel kinds. Alkenes, cyclic alkanes, and aromatics make up kerosene [3]. Despite being widely used in aviation sector, kerosene produced lots of GHG that have a tremendous negative impact on the atmosphere. To overcome this issue, people are currently working to develope decarbonized energy sources. Approximately 12% of the carbon dioxide (CO_2) emissions released by the transportation industry can be attributed to the aviation sector [3]. In 2015, it was reported that around 781 million tonnes of carbon dioxide (CO_2) were released into the environment as a result of transportation [5]. Kerosene is responsible for emitting two greenhouse gases, namely carbon dioxide (CO_2) and sulfur dioxide (SO_2). [6]. Sulfur dioxide (SO_2) is classified as a hazardous emission because it contributes to the formation of acid rain [6]

The search for clean energy sources over fossil fuels for aviation applications is largely influenced by the consequences of kerosene on the environment. There is a lot of promise for using hydrogen and fuel cell technology as primary power. [7,8]. There are lots of researchers regarding hydrogen as hydrogen has positive specific energy properties and also decarbonized source [3,4,9].

There are two primary ways that hydrogen is used in the aviation industry: first, it is used to replace kerosene in large aircraft, and second, it is used in tiny aircraft to power fuel cells instead of jet engines [10].

1.1 The Aim of This Study

The goal of this thesis work is to model a PEMFC for a specific UAV mission profile in accordance with required power demand for the aircraft. The objectives can be summarized as follows:

1. To perform a literature research on studies relevant to the use of fuel cells as the primary power source for UAV applications and the methods used to regulate power output. To develop the PEM fuel cell stack model by integrating required inputs
2. To validate the generated model in accordance with power demand profile for MQ-1 Predator which is defined in [11] by means of simulink tool
3. To define future studies to be conducted to comply with required total power demand

1.2 Literature Survey

Many studies have been conducted to develop fuel cells. Some of them have mainly focused on parameter design and their impact on fuel cell performance and efficency. Some of the research has concentrated on the operational factors and parameters and how they relate to the fuel cell's performance and output power.

In the study [12], under static electrolyte conditions, ion transfer rates (current) for fuel cells of PAFC, PEMFC, SOFC, AFC, and DMFC were investigated in relation to the concentration gradient and electric field. Another crucial factor that negatively impacts system performance is water management. In [13], effect of the air humidification and oxidant spectroscop on liquid water presence in fuel cell stack was investigated.

The steady state performance of a fuel cell is commonly represented by a polarization curve, also known as a V-I curve. This curve demonstrates the correlation between the output current and voltage of the fuel cell stack. The polarisation curve performance demonstrates the intricate correlation between the air composition, humidification, stack temperature, and the interplay of air supply, water management, and cooling process [14].

According to Pukrushpan et al. [15], there are three primary subsystems inside a fuel cell control system that handle:

- Controlling air and hydrogen supply.
- Controlling water exhaust.
- Controlling heat produced.

One of the critical points being used in modelling for fuel cell stack is controlling of the oxidant's flow rate to meet power demand profile. In [16], the study attempted to enhance the response of the system to load variations by implementing a reactant controller, which is a type of feedback control system that adjusts the rate at which reactants are fed to the fuel cell.

The study [17] gives an excellent high-level overview of the economics and climate impact associated with the integration of hydrogen technologies in aviation for different type of unmanned air vehicles.

Another study [18] conducted for overall fuel cell modelling. An examination was conducted on a 3kW PEM fuel cell system's model and control approaches. The study consists includes cooling system, humidifier and manifolds.

Lapena-Rey [19] created a small manned aircraft. Within this study, DC motor and additional devices, such humidifier and compressor, are powered by this system. The necessary oxidant and fuel are supplied by an air compressor and a pressurized hydrogen, respectively. The PEMFCs are used as the only power source throughout the cruise phase; however, during takeoff and ascent, the rechargeable batteries supplement the power produced by the PEMFC. To control power flow, a throttle control is examined. The delayed response of fuel cells is also resolved by this technology.

1.3 Hydrogen in Aviation

Hydrogen is considered as a great alternative to the fuel which are widely used in transportation [20]. Hydrogen is not mature enough to be consiedere as suitable alternative fuel for aviation [21]. Research on alternative fuels for aviation has gained attention because to the recent rapid rise in civil aviation, in addition to the predicted 4-5% yearly increase in traffic over the next few decades [22].

A project called "Cryoplane" looked into hydrogen-powered aircraft [23]. Despite being in its early stages of development, fuel cell technology for aviation is gaining increasing attention from major aircraft manufacturers. Currently, Airbus and Boeing are investigating the prospect of utilizing fuel cell technology to power the diesel-powered APUs on their aircraft. Additionally, other aircraft systems and devices may be powered by fuel cells instead of batteries. They can be employed, for instance, for the purpose of operating landing gear, pressurizing the cabin, illuminating, and providing instruments in the cockpit, as well as for protecting the wings from ice and controlling the surfaces of the aircraft.

Anticipation of an increase in both interest and utilization of fuel cell and hydrogen technology in airplanes is projected. Overcoming significant obstacles such as the expensive technology, hydrogen generation, storage, and refueling systems, aircraft design, and other associated problems could result in the development of a commercial airliner powered by fuel cells in the next 10 to 20 years.

Most of the currently active Unmanned Aerial Vehicles (UAVs) use batteries as their power source because traditional power sources like gas turbines and reciprocating engines are not efficient enough for small-scale vehicles.

However, due to the batteries having a poor energy density, meaning less energy per unit mass, if a longer flying length or improved endurance is required, the weight of the UAV may need to be substantially increased. A potential new power source substitute for current batteries is the fuel cell. Belmonte et al. [24] compared the efficiency of fuel cells and batteries in terms of powering UAVs. The most alluring feature of battery-powered UAVs, according to the authors, is their cost, which is about half that of fuel cells. However, it has been noted that one limitation of battery-powered UAVs is the need to increase the weight of the battery in order to attain a lengthy flight period.

The primary benefits of using fuel cells to power UAVs are their better energy density, which enables longer mission durations and distances, as well as their silent, dependable operation, reduced need for lithium battery charging, and reduced transport difficulties [25]. Because PEMFCs can function at low temperatures, which results in decreased BoP needs, they are chosen for use in UAV applications. AeroVironment created the first fuel cell unmanned aerial vehicle in 2005 [26]. The fifteen-meter-span aircraft was propelled by a PEMFC system and was able to fly for more than an hour only on liquefied hydrogen. Following that in 2006, Bradley et al. [27] created and tested a compressed hydrogen-powered unmanned aerial vehicle (UAV). With a total mass of 16.4 kg and a wingspan of 6.58 m, the authors showed that a 500W PEMFC could power the aircraft. Worldwide research efforts are currently being made to design, develop, and build unmanned aerial vehicles (UAVs) fueled by fuel cells. Due to these efforts, endurance has significantly increased and now exceeds 48 hours [28]. Fuel cell technology will be more appealing to UAVs if it can reduce weight, increase power density, speed up startup, and improve longevity and dependability [29].

Following the 20th century, researchers have also investigated the use of fuel cell technology as a possible energy source for manned aircraft. [9]. In 2008, Boeing Research & Technology Europe (BR&TE) successfully tested the first-ever light piloted aircraft fueled by a fuel cell. [30]. An airplane with a seating capacity of two and a wingspan measuring 16.3 meters, powered by a Proton Exchange Membrane Fuel Cell (PEMFC), has successfully accomplished a 20-minute flight at a velocity of 100 km/h [4]. In 2016, the German Aerospace Center (DLR) created and examined the HY4, a four-seat passenger aircraft that runs on fuel cells [31]. The HY4 aircraft, with a maximum weight of 1500 kg, obtained the required power for takeoff and climb by harnessing electricity from a Proton Exchange Membrane Fuel Cell (PEMFC) with assistance from a lithium battery. The average operational velocity was sustained at 145 km/h.

2. PEM FUEL CELL

The proton exchange membrane fuel cell (is one of the most elegant types of fuel cells in terms of its design and mode of operation It consists of a solid polymeric proton conducting membrane (the electrolyte), which is sandwiched between two platinum catalyzed porous gas diffusion electrodes in a single cell.

PEM fuel cell technology has advanced to a pretty high level of development over the last ten years because to significant expenditures made by the automotive industry [32]. As a fuel, PEM fuel cells typically utilize purified H_2. At the anode, H_2 is oxidized to produce electrons and positively charged H^+ ions. From the anode to the cathode, the positively charged ions travel through the electrolyte. An electric current is generated when electrons exit the electrolyte and traverse the wire that links the anode and cathode. At the cathode, hydrogen ions (H^+) combine with electrons and undergo a reaction with oxygen to produce water (H_2O). The half reactions are provided in equations 2.1 and 2.2. Figure 2.1 depicts a PEM fuel cell illustration.

Half-reaction of oxidation (anode):

$$H_2 \rightarrow 2H^+ + 2e^- \tag{2.1}$$

Half-reaction of oxidation (cathode):

$$O_2 + 4H^+ + 4e^- \rightarrow 2\mathrm{H}_2O \tag{2.2}$$

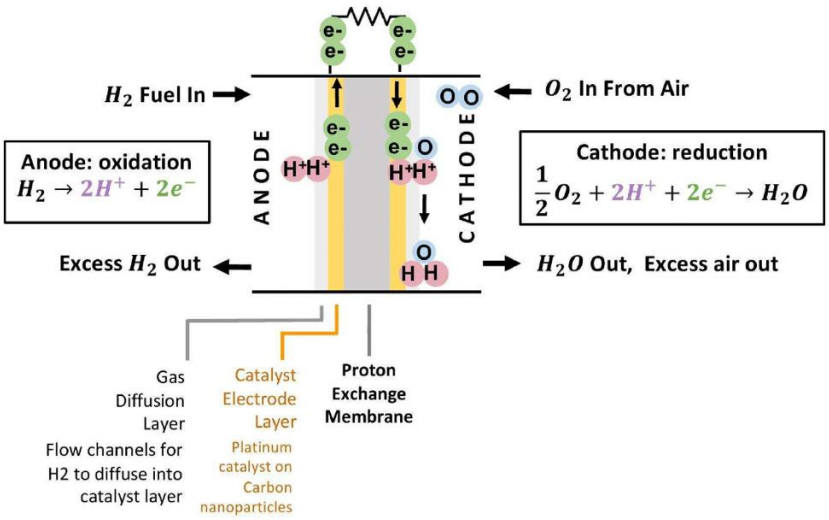

Figure 2.1 : PEM fuel cell working principle [33].

PEM fuel cells are appealing due to their comparatively low operational temperatures. Decreasing temperatures lead to quicker startup times and remove the need for extra balance of plant gear to sustain elevated temperatures. Nevertheless, the typical operational temperatures of approximately 80°C for PEM fuel cells present several challenges.

The rate of oxygen reduction and hydrogen oxidation affects PEM fuel-cell performance. To speed up the reaction at the anode and cathode, platinum is employed as a catalyst. Nonetheless, the cathode's oxygen reduction rate is rather slow [34]. The primary limitation on the efficiency of PEM fuel cells is the slow pace at which the O_2 half reaction occurs, which is more than 100 times slower than the H_2 oxidation half reaction.

Increasing the operating temperature of PEM fuel cells is one way to accelerate reactions and is, to some extent, an option. Polymer electrolyte membranes enable proton exchange membrane fuel cells. The solid organic polymer composing these membranes must be hydrated to allow H^+ ions to pass through. Therefore, it is necessary for PEM fuel cells to function in conditions that ensure the existence of liquid water.

A PEM fuel cell's water concentration requires careful balance in addition to the requirement for liquid water. $H3O^+$ ions travel between polymer sites in the membrane to cause ion mobility. An inadequately permeable membrane hinders the efficient

transmission of H^+ ions, whereas an excessively permeable membrane obstructs the passage of O2 molecules through the surplus liquid water and prevents their access to the catalyst sites. Presently, the existing PEM technology requires that the humidity of a PEM fuel cell should be kept below 100% to prevent the build-up of liquid water in the electrodes. Additionally, it should be maintained above 80% to prevent excessive drying and hinderance of proton conductivity [35]. At operating temperatures exceeding 60°C, it is necessary to humidify the reactant gases to avoid excessive drying of the fuel cell. This humidification demand necessitates the implementation of additional balance of plant equipment.

PEM fuel cells can operate at temperatures exceeding 100 °C under pressure, albeit at the expense of reduced lifespan. Generally, PEM fuel cells with power outputs below 1 kW are operated under normal air pressure, whereas those with power outputs over 5 kW are often run at elevated pressures. Increasing pressures can enhance the performance of fuel cells, however this requires the use of compression equipment, resulting in additional expenses, increased weight, and space constraints.

Utilizing pure H_2 as fuel is another technological hurdle for PEM fuel cells. Sulfur and CO, two impurities that are frequently found in H_2 fuel, attach to the surface of platinum catalysts. As a result, there are fewer platinum catalyst sites accessible for the oxidation of H_2. Temperature affects CO adsorption on platinum catalysts. At 80°C, the performance of cells is considerably reduced by 10 to 20 parts per million (ppm) of CO. Nevertheless, platinum-based catalysts exhibit resistance to as much as 1,000 parts per million (ppm) of carbon monoxide (CO) when exposed to a temperature of 130 °C. Modifying the operational parameters of the electrolyte is required due to the platinum catalyst's tolerance.

The production of H_2 propellant presents unique technical obstacles. Nowadays, the majority of H_2 produced is derived from hydrocarbon resources, most notably methane (CH_4). The technical process of converting hydrocarbon fuels into hydrogen gas is challenging and leads to the creation of carbon dioxide at processing temperatures ranging from 700 to 1000^{o}C. The primary emphasis of conventional technology is the steam reformation of methanol to H_2. H_2, 24% CO_2, 6% N_2, and traces of CO make up around 70% of the final gas mixture [36]. Furthermore, infrastructure for the mass transportation of H_2 fuel has not been constructed.

Heat is generated during the conversion of chemical energy to electrical energy in a fuel cell. The amount of heat produced and the method required for its removal impact the fuel-cell system's balance of plant requirements. Reactant air flow can be used to cool PEM fuel cell stacks with power outputs below 100 watts. However, stacks with power outputs ranging from 100 watts to 1 kW require their own air-cooling systems, which may include pumps or blowers. Water cooling systems are necessary for PEM fuel cell stacks that have a power output exceeding one kilowatt. Incorporating a separate cooling system, such as water or air-cooled, significantly enhances the requirements of the balance of plant for the fuel cell.

For PEM fuel cells to become a feasible choice for energy production, they must contend with existing technologies. The current efficiency of PEM fuel cell devices ranges from 40 to 60 percent. [37]. The utilization of H_2 as a fuel in a PEM fuel cell yields a maximum theoretical efficiency of 83%, as determined by Gibbs free energy [38]. About 0.7 volts are produced by a present PEM unit cell. At 80 °C and 1 atmosphere, an ideal H_2/air unit cell should deliver 1.16 volts.

2.1 PEM Fuel Cell Components

The components that make up a fuel cell system each have distinct functions and characteristics. While exchanging protons and water, the polymer membrane acts as an electric insulator. On the catalyst surface, electrochemical processes take place. In addition, the catalyst needs to have pores for the transportation of water as well as media that conducts electrons and protons. The gas diffusion layer provides holes for water movement, electrically conductive pathways for electric conduction, and uniform distribution of reactant gases across the fuel cell active surface.

2.1.1 Membrane

In PEM fuel cells, the electrolyte that supplies ions for proton transfer is polymer membrane. The membrane must handle high currents with minimal resistive losses and strong proton conductivity in order to be utilized in PEM fuel cells. In order to create electricity, electrons need to be compelled to travel via an external circuit, while ensuring that the anode and cathode compartments are electrically separated. When in use, the barrier should effectively prevent the fuel and oxidant gasses from mixing, as long as it possesses sufficient mechanical strength and stability [39,40].

Nafion, made by DupontTM, is one of these several membrane types that has become the industry standard. Nafion serves as the benchmark for any newly developed membrane due to its high proton conductivity and long lifespan, qualities that led to its replacement of other membrane types [40].

The water absorption ratio, defined as the proportion of water molecules to sulfonic acid groups, significantly influences the proton conductivity of Nafion. However, it is best to avoid having too much water in the system since this could clog the catalyst's pores and the gas diffusion layer, making it impossible for gases to reach the reaction sites. Additionally, it has been noted that dryness causes the membrane's proton conductivity to drop above 80°C; therefore, the membrane temperature should be maintained between 60 and 80°C to avoid this phenomena in the system [41]. Thus, it may be inferred that in order to preserve the membrane's elevated proton conductivity and functionality, the control system must effectively manage both temperature and water content.

2.1.2 Catalyst

The electrodes that are present at the anode and cathode of the membrane for the reactions involving hydrogen oxidation and oxygen reduction, respectively, are known as catalysts. PEM fuel cell catalyst should include pores that permit the transfer of reactant gas and water, in addition to providing active sites for reactions and satisfying both proton and electron conductive routes. Because of their high electrocatalytic activity and resistance to corrosion and oxidation, Pt and alloys supported by Pt are frequently utilized in PEM fuel cells. Yet because Pt is an expensive metal, a sizable portion of the stack cost is made up of it. Studies utilizing smaller particles over time reduce Pt loading by optimizing surface area and increasing Pt utilization efficiency. Numerous studies have also looked into various precious, non-precious, and integrated metals in an effort to lower the cost of catalysts [42, 43].

Pt is often distributed on carbon support; this support material needs to be strong in corrosive conditions, have a large surface area, and be electrically conductive in order to facilitate the flow of electrons. Nafion is commonly used as a binder in catalyst preparations and is added to proton conduction membranes. Catalyst particles can have hydrophobic materials, such as polytetrafluoroethylene (PTFE), added to them to make dry spots where reactant gas can pass through. In order to reduce transport losses, it is necessary to optimize the distribution of Pt, carbon, Nafion, and PTFE, and

maximize the ternary phase boundaries [43]. There are two distinct approaches to MEA preparation. The membrane between the two layers may be squeezed once the catalyst has been added to the gas diffusion layer. Second, the catalyst can be pressed straight into the membrane using GDLs [44]. For reduced possible losses, the contact resistance between the catalyst and membrane should be kept to a minimum.

2.1.3 Gaz diffusion layer

The porous diffusion medium known as the "gas diffusion layer" is what evenly distributes reactant gases across the fuel cell's active region. It is positioned on the anode and cathode, between the bipolar plates and the catalyst layer. In order to transmit heat produced by catalysts to other fuel cell components, GDL needs to be both thermally and electrically conductive. The most common GDLs are carbon paper and carbon fabric. Water is handled within the MEA by employing hydrophilic and hydrophobic (PTFE Teflon) additives in GDLs. The hydrophilic GDL channels carry the water generated at the catalyst surface to the output gas channels. Thus, species transport is unimpeded and reactant gases follow the hydrophobic channels [45, 46]. Effective water management is necessary to keep gas transport running and prevent flooding.

2.1.4 Bipolar plates

In fuel cell systems, bipolar plates have multiple purposes. They allow electron transfer to complete the circuit because they are electrically conductive. They create a stack of individual cells connected in series by joining the anode of one cell to the cathode of the next cell. Since these plates support the MEA structurally, they ought to be strong and long-lasting. They supply a flow field along with fuel and oxidant fluxes. To ensure that the reactants follow the gas pathways and arrive to GDL, they must be impermeable to gases. Bipolar plates should have strong thermal conductivities since they also provide stack cooling through the cooling channels. Lightweight materials are desired because the bipolar plate weight makes up the largest percentage of the stack weight. The material must to be inexpensive to produce and simple to machine. It must endure the fuel cell's corrosive environment [45].

Metals, polymer-graphite composites, and graphite are the materials utilized to make bipolar plates. Graphite exhibits strong electrical conduction and chemical stability, but mechanical durability is lacking because of its brittle structure. Furthermore, the

technique of creating flow fields on graphite plates through machining is costly. Graphite is additionally strengthened mechanically by the use of certain polymer compounds. These polymers increase the flexibility of the plates without compromising their chemical stability, but they also reduce graphite's electrical conductivity.

Metals are stronger mechanically and have superior electric conduction, but they corrode easily in the fuel cell's acidic environment. To solve this issue, several coating materials are applied without lowering electrical conductivity [47].

2.1.5 Reactant supply

Reactants must be supplied to the system in proper proportions to ensure a consistent power output. The regulation of fuel and oxidant supply should minimize excess reactants and reduce parasitic losses from power-supplying equipment. By carefully controlling the fuel supply, lower reactant partial pressures can be achieved, preventing undersupply of reactants. Reactant starvation, resulting from inadequate gas supply, sudden load increases, and fuel cell startups, negatively affects the longevity and reliability of fuel cells. Catalysts deteriorate due to fuel starvation-induced voltage reversals. Other processes seen in fuel-starving fuel cells include water electrolysis, carbon corrosion, and Pt or Ru dissolutions. During fuel starvation, measurements on the active area of the fuel cell also indicate uneven voltage and current distributions [48]. Oxidant deficiency leads to decreased reaction rates and current densities, as well as rapid cell reversals [49].

In order to provide hydrogen, pressurized containers or hydrogen reformers may be utilized. Since the use of reformate gas limits catalyst performance and durability, pressurized hydrogen tanks offer a better hydrogen supply for control experiments. Air is typically employed in fuel cells as an oxygen source. Compressors, blowers, etc. could be used to meet the need for air. Filters and leak-proof lubrication systems should be installed on the air supply equipment to lessen the chance of contamination. They also need to respond quickly to changes in load [50].

To rapidly regulate the passage of hydrogen from a source of extremely high pressure, Pukrushpan et al. devised a valve. The valve is opened in accordance with the pressure differential between the cathode and anode manifolds. A simple proportional controller is used to lessen the pressure difference between these arrangements. To

keep the anode and cathode pressures equal, the controller employs pressure difference feedback [51].

Within [52], feed-forward control method is integrated for the air supply. The oxygen stoichiometry and stack current are used to determine the input voltage of the compressor motor. The disturbance is removed by utilizing a feed-forward compensator and measuring the necessary current. The control signal from the compensator then activates the centrifugal compressor.

2.1.6 Cooling system

Maintaining a specific stack temperature has a big impact on how safely and effectively fuel cells operate. Excessive loss of heat can lead to stack overheating, resulting in considerable dehydration of the polymer membrane. This would result in a significant increase in resistance and a decrease in proton conductivity. Due to drying out at high temperatures, cells positioned at the middle of the stack are particularly susceptible to abrupt voltage decreases. Another thing to consider is that hot spots created by high temperatures can result in membrane leaks. Because of the leaks, which allow hydrogen and oxygen to combine, this condition may lead to dangerous positions [53]. The fuel cell stack requires a cooling system that effectively reduces unnecessary losses and eliminates excessive heat at any level of stack current, thus ensuring that the stack temperature remains at the appropriate level. This will help to avoid membrane leaks and performance losses. A proportional feedback controller for temperature regulation was created by Vega-Leal et al. [52]. This study presents a fuel cell system that utilizes air cooling and incorporates a fan to cool the stack. This work's cooling method involves employing a proportional controller to change the fan speed in response to a temperature differential between the target and stack.

3. AUXILIARY EQUIPMENT MODELLING

3.1 Compressor Model

The components of the compressor model are the map of the compressor, the compressor itself, and the motor inertia, as shown in Figure 3.1. Depending on the required pressure, motor speed, and power, the airflow rate is defined by the fixed values in the compressor map. The flow rate is determined by the compressor map, which takes into account the inertia of the motor and compressor to establish the compressor speed.

The compressor speed is defined by the second portion, which also represents the inertia of the motor and compressor. Therefore, the compressor map uses the velocity to calculate the rate at which air mass flows. Since the incoming air is normally atmospheric, it is assumed that its temperature and pressure are fixed at T_{atm} = 25°C and P_{atm} = 1 atm, respectively.

The motor command is one of the inputs to the fuel cell system. The supply manifold model is used to ascertain the pressure downstream. A compressor flow map is utilized to compute the air mass flow rate of a compressor by considering its speed and pressure ratio.

The inertia of the compressor and motor dictate the operating speed of the compressor, which in turn governs the flow rate in the compressor map. Equation 3.1 describes the dynamics of the compressor speed, w_{cp}(rad/sec), where J_{cp} (kg.m2) is the total inertia of the motor and compressor, τcm (N.m) is the torque applied to the compressor motor, and τcp (N.m) is the torque that the compressor requires. [51]

$$J_{cp}\frac{d\omega_{cp}}{dt} = \tau_{cm} - \tau_{cp} \tag{3.1}$$

Equation 3.2 gives the motor input torque using as motor constants (k_t R_{cm}, k_v), with ηcm representing the motor's mechanical efficiency.

$$\tau_{cm} = \eta_{cm}\frac{k_t}{R_{cm}}\left(v_{cm} - k_v\omega_{cp}\right) \tag{3.2}$$

Equation 3.3 gives the torque that the compressor needs as

$$\tau_{cp} = \frac{c_p}{\omega_{cp}} \frac{T_{atm}}{\eta_{cp}} \left[\left(\frac{P_{sm}}{P_{atm}} \right)^{\gamma - \frac{1}{\gamma}} - 1 \right] W_{cp} \tag{3.3}$$

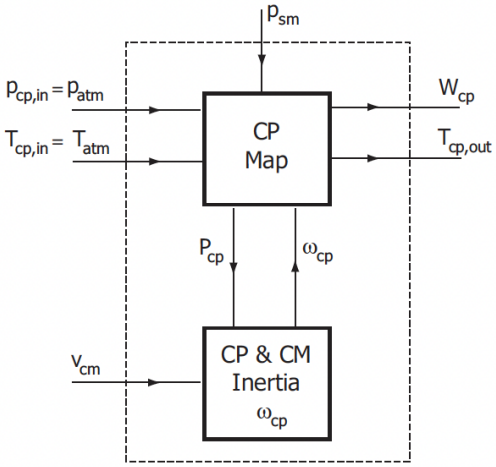

Figure 3.1 : Compressor block diagram.

A compressor model attached in the model which is generated in the light of the information outlined above is illustrated in Figure 3.2.

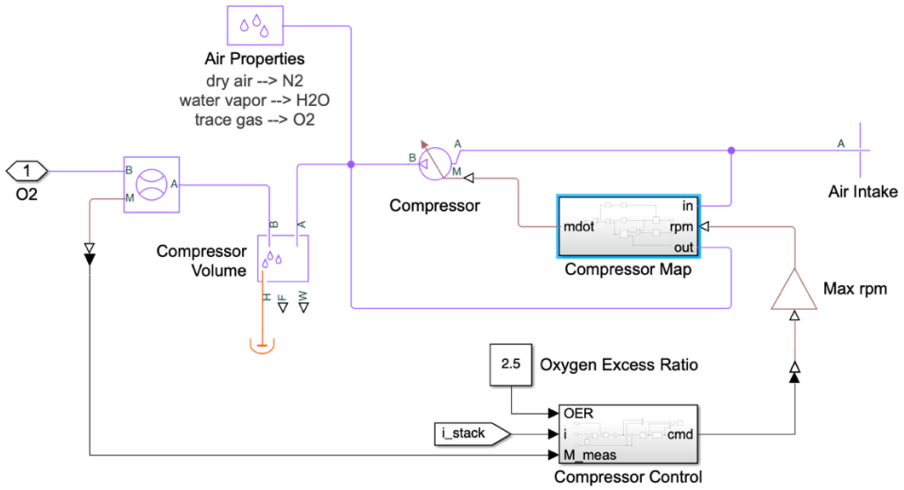

Figure 3.2 : Compressor model in the study.

3.2 Humidifier Model

As shown in Figure 3.3**Hata! Başvuru kaynağı bulunamadı.**, the humidifier's air stream is injected with water to make it more humid before the cooler's output reaches the stack. Given the small size of the humidifier in this case, it can be considered as part of the overall volume of the supply manifold. The difference in air humidity

caused by the extra water input is computed using a static model of the humidifier. It is assumed that the temperature of the flow remains constant and that the latent heat of vaporization is provided by either the injected water in the form of vapor or the air cooler.

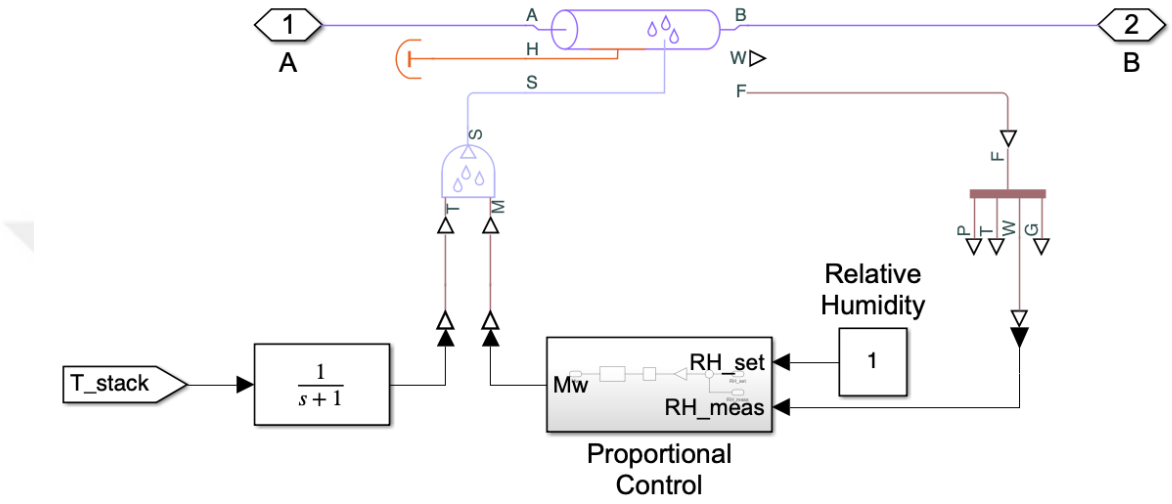

Figure 3.3 : Humidifier model.

Calculating the dry air pressure $P_{a,cl}$, vapor mass flow rate $W_{v,cl}$ and dry air mass flow rate Wa,cl using the thermodynamic properties is possible depending on the flow state exiting the cooler ($W_{cl} = W_{sm,out}$, P_{el}, T_{el},$Ø_{cl}$). The vapor saturation pressure, considering the flow temperature, is calculated using equation 3.4. Then, we use equation 3.5 to determine the vapor pressure [51].

$$\rho_{v,cl} = \phi p_{sat}(T_{cl}) \tag{3.4}$$

$$\phi = \frac{p_v}{p_{sat}} \tag{3.5}$$

Where:

p_v= the mixture's water vapor pressure

p_{sat}= vapor saturation pressure at the mixture's temperature

Humid air can be described as a combination of dry air and vapor. The partial pressure of the dry air is calculated by subtracting the vapor pressure from the total pressure:

$$\rho_{a,cl} = p_{cl} - \rho_{v,cl} \tag{3.6}$$

Next, the humidity ratio can be computed by using:

$$\omega = \frac{M_v}{M_a} = \frac{\rho_{v,cl}}{\rho_{a,cl}} \tag{3.7}$$

where M_a is the molar mass of dry air (28.84×10^{-3} kg/mol).

The cooler's mass flow rate of vapor and dry air is

$$W_{a,cl} = \frac{1}{(1 + \omega_{cl}} \, W_{cl} \tag{3.8}$$

$$W_{v,cl} = W_{cl} - W_{a,cl} \tag{3.9}$$

At the humidifier's input and outflow, the mass flow rate of dry air is constant $W_{v,cl} = W_{a,cl}$. Injecting more water increases the pace at which water vapor flows:

$$W_{v,hm} = W_{v,cl} + W_{v,inj} \tag{3.10}$$

Additionally, the vapor pressure varies, and equation 3.11 can be used to compute it.

$$\omega = \frac{m_v}{m_a} = \frac{\frac{\rho_v V}{R_V T}}{\frac{\rho_a V}{R_a T}} = \frac{R_a p_v}{R_v p_a} = \frac{M_v}{M_a}\frac{p_v}{p_a} \tag{3.11}$$

$$p_{v,hm} = \omega_{cl}\frac{M_a}{M_v}\,\rho_{a,cl} = \frac{W_{v,hm}}{W_{a,cl}}\frac{M_a}{M_v}\,\rho_{a,cl} \tag{3.12}$$

The overall pressure rises as a result of the rising vapor pressure. The mass continuity controls the humidifier's exit flow rate:

$$W_{hm} = W_{a,cl} + W_{v,hm} = W_{a,cl} + W_{v,cl} + W_{v,inj} \tag{3.13}$$

3.3 Cooling System Model

Irreversibilities will result in the production of heat during energy generation by the fuel cell stack. A cooling system needs to be run in order to maintain the system temperature at the intended setpoint. A variety of system-integrated cooling devices can be used to achieve cooling. The cooling system under consideration in this work, consisting of a fan and a cooling water pump coupled to a radiator, is used to derive the corresponding model. Figure 3.4 illustrates how the cooling water is routed through the bipolar plate stack's machined water channels and back to the radiator.

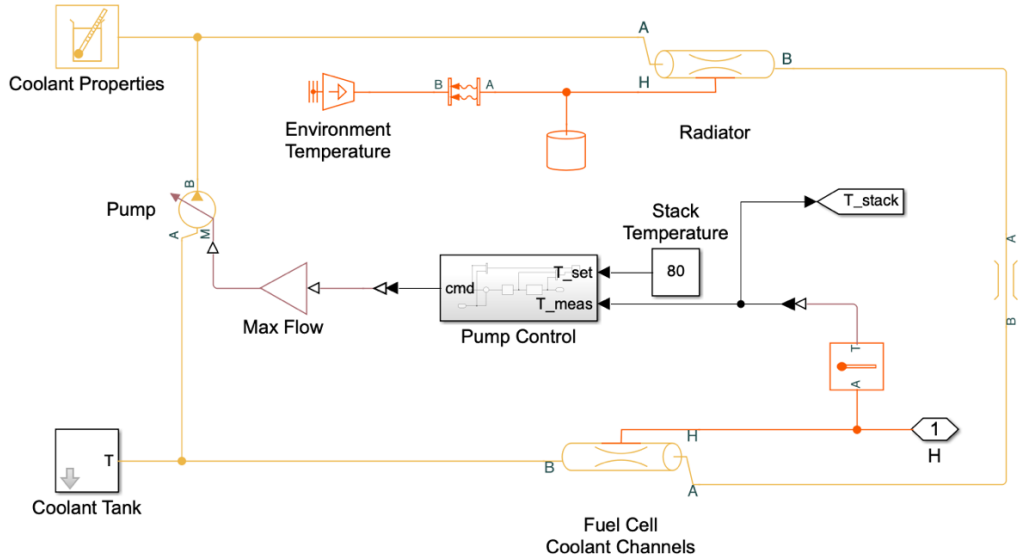

Figure 3.4 : Cooling system model.

The radiator's contents are the definition of the system used to construct cooling system modeling equations. Equation 3.14 represents the mass balance for cooling water, where $\dot{m}_{in}$ indicates that hot water is entering the radiator from the stack, $\dot{m}_{out}$ is the amount of water still in the radiator after cooling, and m_r is the total volume of water in the radiator.

$$\dot{m}_{in} - \dot{m}_{out} = \frac{dm_r}{d_t} \tag{3.14}$$

The value described is the constant that equation 3.15 will uphold due to the presence of water in the radiator upon installation. Consequently, the mass accumulation terms will decrease, as shown by equation 3.16.

$$\dot{m}_{in} = \dot{m}_{out} = \dot{m} \tag{3.15}$$

$$\frac{dm_r}{d_t} = 0 \tag{3.16}$$

Equation 3.17 can be used to determine the water flow rate based on the voltage and pump characteristics.

$$\dot{m} = \dot{m}(V_{pump}) \tag{3.17}$$

Equation 3.18 outlines the overall energy balance for the radiator, assuming that the physical constants remain constant and disregarding any contributions from kinetic and potential energy.

$$Energy_{in} = Energy_{out} - Energy_{accumulation} \tag{3.18}$$

Energy removal occurs when cold water leaves the stack and heat is transmitted from the radiator surface to the environment, as shown in equations 3.19 and 3.20, where intake energy is the amount of heat that the radiator takes in from the stack.

Equation 3.21 provides the energy accumulation term for the radiator's contents.

$$Energy_{in} = \dot{m}_{in}\mathrm{H}_{in} = \dot{m}_{in} cp_{water} T_{in} \tag{3.19}$$

$$Energy_{out} = \dot{m}_{out}\mathrm{H}_{out} + Q_{removed} = \dot{m}_{out} cp_{water} T_{out} + uA\Delta T_{lm} \tag{3.20}$$

$$Energy_{accumulation} = \frac{dU}{dt} = V_{rad} p\ cp_{water} \frac{d(T - T_{ref})}{dt} = V_{rad} p\ cp_{water} \frac{dT}{dt} \tag{3.21}$$

The symbol Cp_{water} (J/ (kg. K)) stands for water's thermal capacity, T (K) represents the temperature, u (W/(m^2.K)) denotes the overall heat transfer coefficient, A (m^2) depicts the radiator's surface area for heat transmission, and ρ (kg/m^3) represents the density of water. Equations 3.15–3.21, instead, might be used to rewrite equation 3.19 as equation 3.22.

$$m\,(V_{pump}) cp_{water}(T_{in} - T_{out}) - uA\Delta T_{lm} = V_{rad} p\ cp_{water} \frac{dT}{dt} \tag{3.22}$$

The system temperature can be calculated by averaging the input and output temperatures of the radiator, as shown in equation 3.23.

$$\frac{dT}{dt} = \frac{1}{2}\left(\frac{dT_{in}}{dt} + \frac{dT_{out}}{dt}\right) \tag{3.23}$$

Assuming a constant ambient air temperature (K), the log-mean temperature can be calculated using equation 3.24 [54].

$$\Delta T_{lm} = \frac{(T_{\infty} - T_{out}) - (T_{\infty} - T_{in})}{\ln(\frac{(T_{\infty} - T_{out})}{(T_{\infty} - T_{in})}} \tag{3.24}$$

Consequently, the variable "u" can be approximately represented as a mathematical function of the voltages applied to the pump and fan, as shown in equation 3.25. The overall heat transfer coefficient is determined by the water and air flow rates, which are related to the pump and fan voltages.

$$\cup = \cup \left(V_{fan}, V_{pump}\right) \tag{3.25}$$

Equation 3.26 represents the general energy balance, which is obtained by combining equations 3.22–3.25.

$$m\left(V_{pump}\right)cp_{water}(T_{in} - T_{out}) - (\cup \left(V_{fan}, V_{pump}\right)A\frac{(T_{\infty} - T_{out}) - (T_{\infty} - T_{in})}{\ln(\frac{(T_{\infty} - T_{out})}{(T_{\infty} - T_{in})}} = V_{rad}p\ cp_{water}\frac{1}{2}\left(\frac{dT_{in}}{dt} + \frac{dT_{out}}{dt}\right) \tag{3.26}$$

Equation 3.27 gives the following integration with the cooling system and stack:

$$\frac{dT_{st}}{dt} = \dot{Q_{generatıon}} - Q_{removed} \tag{3.27}$$

3.4 Recirculation Model

Anode recirculation is a process that redirects the hydrogen flow from the exit to the anode inlet in order to make use of the remaining hydrogen [55]. This is similar to the P2000 system. This recirculation enhances system efficiency by augmenting the utilization of hydrogen in steady-state conditions.

Fuel cell stacks receive hydrogen after going through multiple phases of pressure reduction and a humidifier. The hydrogen supply system in this air vehicle is a closed circuit. Using an ejector jet pump that takes advantage of the pressure drop created by hydrogen consumption in the stacks, hydrogen recirculation is carried out passively. Figure 3.5 illustrates the schematic of the ejector that is being used on the system model for recirculation purposes.

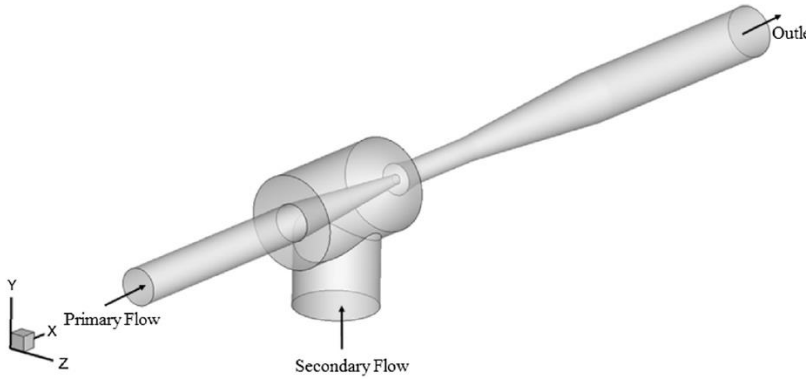

Figure 3.5 : Schematic of the ejector.

Equation 3.28, this comes from energy balance and isentropic flow laws [56], yields the nozzle throat diameter D_{nt}

$$m_p = pA_m(\zeta \kappa R_g T\left(\frac{2}{\kappa+1}\right)^{\frac{\kappa+1}{2(\kappa-1)}} \tag{3.28}$$

The mass flow rate of the primary flow, denoted as m_p, is calculated using equation 3.28. where Ant (equals to $pD_{nt}^2/4$), n, R_g, and κ are the nozzle throat area, initially, the isentropic coefficient, then the gas constant, and finally, the specific heat ratio of the gas in the main flow.

$$m_p = \frac{N_{cell} I M_{H2}}{2F} \tag{3.29}$$

Where F is Faraday's constant, N_{cell} is the PEMFC stack's cell number, I is current, and M_{H2} is hydrogen's molecular weight. The diameter D_{nt} and nozzle throat area A_{nt} are determined when the equation's previously stated parameters in equation 3.28 are known. Figure 3.6 shows the schematic with the recirculation model integrated into the research.

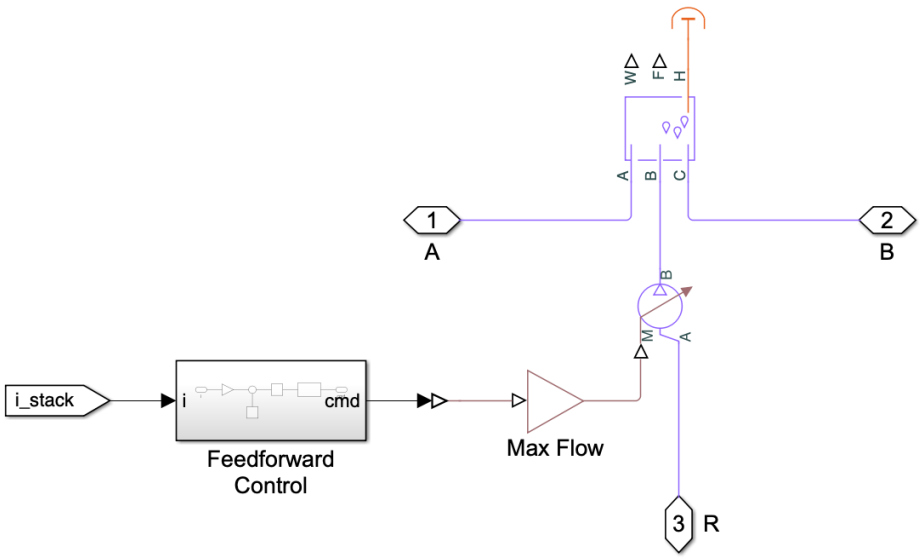

Figure 3.6 : Schematic of recirculation model.

4. FUEL CELL STACK MODELLING

4.1 Stack Voltage Model

The stack voltage model computes the stack voltage based on the stack current and estimates the losses experienced in the polarization curve. The literature contains a variety of models for calculating a cell's voltage in relation to current, temperature, humidity, and chemical partial pressures.

A hydrogen/oxygen fuel cell with a liquid water product has an ideal standard potential of 1.229V at standard state conditions (250 ^{0}C and 1 atm). Irreversible losses lead the real cell potential to fall below its equilibrium potential, nevertheless. There are three types of irreversible losses: activity losses, concentration losses, and ohmic losses. The probable cell death at low current density is nearly entirely caused by the activation losses of the oxygen reduction pathway. The concentration losses, however, grow in magnitude with increasing current densities. The voltage output of a single cell can be calculated using equation 4.1. which uses an empirical equation derived by Amphlett et al. [57] and Kim et al. [58] to determine the PEMFC output characteristics.

$$V_{cell} = E_{Nerst} - V_{act} - V_{ohm} - V_{con} \tag{4.1}$$

4.2 Anode Flow Model

A hydrogen canister stores compressed hydrogen as part of the technology being discussed. Given the high-pressure storage, it's reasonable to expect a valve to swiftly adjust the anode's inflow flow rate in order to keep the cathode-anode pressure differential as low as possible. In short, we believe that there is enough flow of hydrogen as long as the pressure differential is maintained and there is a minimal difference between the anode channel flow resistance and the cathode flow resistance. There are other assumptions that are similar to the model of cathode flow. The flow temperature and the stack temperature are taken to be equal. It is anticipated that the gas in the anode flow channel will have the same pressure, temperature, and humidity as the anode output flow. One volume also contains the backing layer and flow channel for all cells [51]. Anode flow model is defined in Figure 4.1

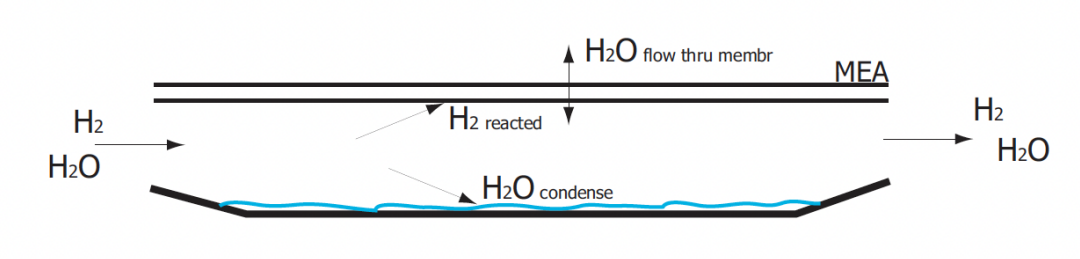

Figure 4.1 : Anode mass flow. (Pukrushpan J.T,2004:41)

In the anode volume, water may be vapor or liquid. Equation 4.2 illustrates how to apply the ideal gas law to determine the maximum vapor in the anode, assuming equal vapor phase and anode volumes. Here, P_{sat} (P_a) represents the saturation pressure from equation 4.3, V_{anode} (m^3) the anode volume, M_{H2O} (kg/mol) the molecular weight of water, T_{stack} (K) the stack temperature, and R, 8.314 $J.mol^{-1}.K^{-1}$, is the ideal gas constant.

$$m_{vapor,max.anode} = \frac{P_{sat} V_{anode} M_{H_2O}}{RT_{stack}} \tag{4.2}$$

$$logP_{sat} = -1.69x10^{-4}T^4 + 3.85x10^{-7}T^3 - 3.39x10^{-4}T^2 + 0.143T - 20.9 \tag{4.3}$$

Liquid water will occur as indicated by equation 4.4 if the anode compartment's water content surpasses the maximum permitted vapor level.

$$m_{H20liq,anode} = m_{H20.anode} - m_{vapor,max.anode} \tag{4.4}$$

Equation 4.5 states that the total pressure in the anode volume is the sum of the partial pressures for hydrogen and vapor, which are found in equations 4.6 and 4.7, respectively.

$$P_{anode} = P_{H2,.anode} + P_{vapor,.anode} \tag{4.5}$$

$$P_{anode} = \frac{m_{H20.anode}}{V_{anode M_{H2}}} RT_{stack} \tag{4.6}$$

$$P_{wapor,.anode} = \frac{m_{vapor.anode}}{V_{anode M_{H2}}} RT_{stack} \tag{4.7}$$

Equation 4.8 expresses the anode's relative humidity, while equation 4.3 estimates the saturation pressure, which is a temperature-dependent function [51].

$$\phi_{anode} = \frac{P_{vapor,.anode}}{P_{sat(T_{stack})}} \tag{4.8}$$

Equations 4.9–4.13 can be used to determine the hydrogen and vapor inlet flow rates given the known anode inlet humidity, temperature, and pressure.

$$P_{vapor,.anodein} = \phi_{anodein} P_{sat} T_{stack} \tag{4.9}$$

$$P_{H2,.anodein} = P_{anodein} - P_{vapor,.anodein} \tag{4.10}$$

$$w_{anodein} = \frac{M_{H2O}}{M_{H2}} \frac{P_{vapor,.anodein}}{P_{anodein}} \tag{4.11}$$

Where w_{anode} in is the humidity ratio (kg/kg).

$$W_{H2,.anodein} = \frac{1}{1 + w_{anodein}} w_{anodein} \tag{4.12}$$

$$W_{vapor,.anodein} = W_{anodein} - W_{H2,.anodein} \tag{4.13}$$

According to Faraday's law, as shown in equation 4.14, the quantity of hydrogen used up in the process, $W_{H2reacted}$ (kg/s), is known. F is the Faraday's constant, which is 96485C, and n is the number of cells in the stack. I, or amper, is the current.

$$W_{H2,.reacted} = \frac{nI}{2F} M_{H2} \tag{4.14}$$

The anode outlet stream's hydrogen and vapor content can be computed using equations 4.15–4.17.

$$w_{anodeout} = \frac{M_{H20}}{M_{H2}} \frac{P_{vapor,.anode}}{P_{h2,.anode}} \tag{4.15}$$

$$W_{H2,.anodeout} = \frac{1}{1 + w_{anodeout}} w_{anodeout} \tag{4.16}$$

$$W_{vapor,.anodeout} = W_{anodeout} - W_{H2,.anodeout} \tag{4.17}$$

4.3 Cathode Flow Model

The cathode flow model is associated with the electrochemical mechanisms that control the cathode volume's air flow. The cathode compartment is chosen to operate in through flow mode for this study, allowing the oxygen-depleted air to travel via the exit manifold. The technique of the cathode flow model is identical to that of the anode flow model; Faraday's law and ideal gas law complete the mass balances the cathode species.

A number of assumptions are established. At first, it is thought that all gases act like ideal gases. The fuel cell stack's cooling system can maintain a constant temperature of 80°C throughout the stack thanks to its precise temperature control capabilities. Furthermore, it is thought that the temperature of the stack and the flow within the cathode flow channel are equal. Cathode flow model is provided in Figure 4.2.

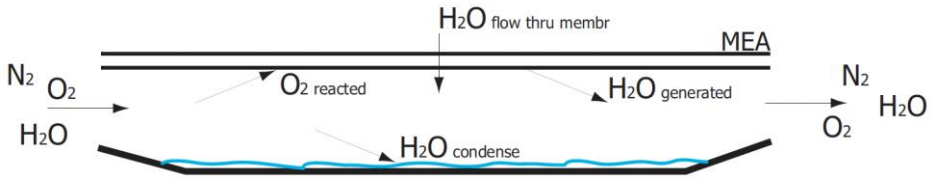

Figure 4.2 : Cathode mass flow. (Pukrushpan J.T,2004:37)

Moreover, vapor turns into a liquid when the cathode gas's relative humidity rises above 100%. The liquid water is present in the stack and has the potential to either vaporize into the cathode gas or accumulate in the cathode when the gas humidity falls below 100%, therefore the spatial variances are not taken into consideration.

According to Faraday's law, the quantities of oxygen consumed and water created by the electrochemical reactions taking place in the system are given by Equations 4.18 and 4.19, respectively.

$$W_{O2,.reacted} = \frac{nI}{4F} M_{O2} \tag{4.18}$$

$$W_{O2,.cathodegenerated} = \frac{nI}{2F} M_{H20} \tag{4.19}$$

Equation 4.20, where i stands for oxygen, nitrogen, and vapor, can be used to express the partial pressures of these three elements in the cathode volume.

$$P_{i,.ca} = \frac{m_{i,.ca}\, RT_{stack}}{V_{cathode} M_i} \tag{4.20}$$

The uniformity assumption states that the cathode outlet pressure equals the cathode pressure. As per equation 4.21, this is equal to the combined pressures of the individual species in the cathode volume.

$$P_{ca} = P_{ca,.out} = \sum P_{i,.ca} \tag{4.21}$$

A basic orifice equation, represented by equation 4.22, may be used to express the oxygen, nitrogen, and vapor cathode exit flow rates. The symbols for cathode and

return manifold pressures, respectively, are P_{ca} and P_{rm},while $k_{ca,out}$ is the orifice constant.

$$W_{ca,.out} = k_{ca,.out}(P_{ca} - P_{rm}) \tag{4.22}$$

The anode flow model's equations can be used in a similar manner to compute the mass fluxes at the cathode's inlet and exit.

5. ANALYSIS AND SIMULATION

Reactant supply systems, including air flow control, hydrogen feed from a high-pressure tank, and reactant feed humidification, are the main focus of the system model development in Chapters 3 and 4. The main source of heat in a direct hydrogen system is the fuel cell. As a result, the reactant systems consider the stack temperature as a target value. The control inputs consist of the instructions for the humidifier water injection, the hydrogen valve, and compressor motor's voltage. A proportional controller for the valve of the hydrogen tank and a static controller for the humidifier have been incorporated into the model in this chapter to enhance it. Table 5.1lists the parameters of the model. Since it will be the main source of motor power and must physically fit inside the limits of the small diameter, highly aerodynamic, high aspect ratio airframe, a fuel cell system with a high power density is necessary. The power requirement of almost 80 kW will also be met by the usage of a liquid-cooled PEMFC. Because the additional parasitic current draw was preferred because of the related mass and volume benefits, hydrogen fuel will be kept in liquid form and oxidant will be supplied via an air-breathing design using a compressor, depending on the endurance and altitude needs of the aircraft. The aircraft's thermal signature will be less noticeable while it is in flight due to the fuel cell system's lower exhaust temperature. Furthermore, the fuel cell's vibration-free, quiet operation will reduce noise pollution. These two fuel cell properties contribute to the low observability that is ideal for reconnaissance missions. Figure 5.2 illustrates a hypothetical flight plan for a MQ-1 Predator conducting a reconnaissance mission with an eight-hour loiter duration above the target location. The calculation of current demand is predicated on producing the entire required power at a nominal voltage of 300V [59]. Control methodologies being integrated to the system to meet aircraft power demand is outlined in Figure 5.1.

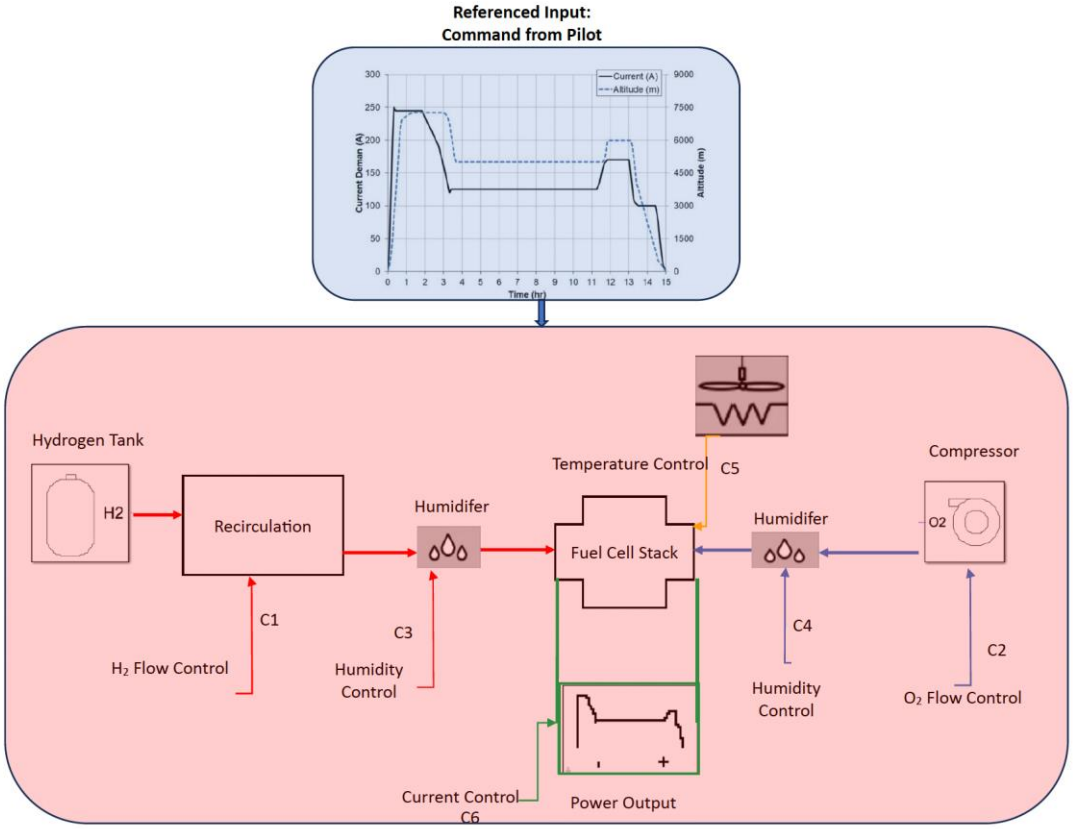

Figure 5.1: System inputs and outputs required for control.

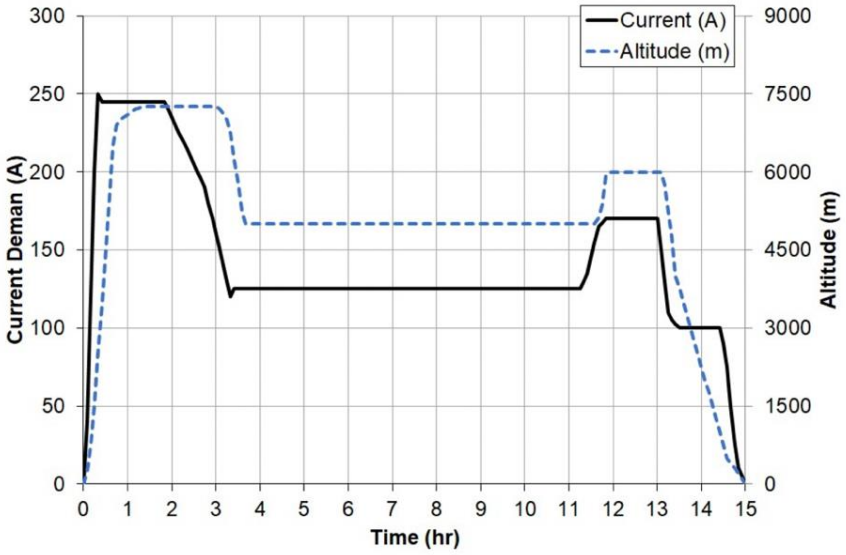

Figure 5.2 : Theoretical profile for MQ-1 Predator UAV. (Thirkell, Alex. 2021:175)

Table 5.1 PEM operational parameters (Spiegel, Colleen,2008).

Parameter	Symbol	Value	Unit
Stack Temperature	t_stack	80	ºC
Membrane Thickness	t_membrane	0.125	mm
Anode GDL thickness	t_gdl_A	0.250	mm
Cathode GDL thickness	t_gdl_C	0.250	mm
Cell Area	stack_area	280	cm^2
Exchange Current Density	I_0	0.0001	A/cm^2
Limiting Current Density	I_L	1.4	A/cm^2
Charge Transfer Coefficient	alpha	0.5	-
Density of Dry Membrane	rho_membrane	2000	kg/m^3

5.1 Controls for Reactant Flow and Humidifier

It is critical to establish controls for the anode hydrogen valve and humidifier in order to prioritize the investigation of air supply dynamics. Thermodynamic calculations suggest that proportional control methodology is preferred on both the anode and cathode sides, as the proportional controller can reduce transient effects and make it relatively simple to control the water injection to achieve the desired humidity

5.1.1 Humidifier control

A fuel cell stack's water production is a function of power level and stack current. As a result, the quantity of vapor that must be introduced to its inlet reactions varies. Specifically, the stack current, ambient air temperature, and humidity all affect how much water vapor is required at the humidifier. Assuming the intake air is at 0% RH and 80 °C, the cathode inlet reactants must be supplemented with the appropriate vapor transfer rate to maintain a membrane relative humidity of 100%.

The quantity of water injected into the air flow $W_{v,inj}$ is assumed to be precisely what is needed to sustain the desired humidity at the inlet of the stack ϕ^{des} in the humidifier. This amount can be computed using the humidifier inlet flow conditions, which correspond to the cooler exit flow.The flow rate W_{cl}, temperature T_{cl}, humidity ϕ_{cl}, and pressure p_{cl} are all part of the inlet condition. We can compute the dry air pressure

$p_{a,cl}$, the vapor mass flow rate $W_{v,cl}$ and the dry air mass flow rate $W_{a,cl}$ using equations 3.4 to 3.9. Next, the injected vapor flow rate is computed using

$$W_{v,.inj} = \frac{M_v}{M_a} \frac{\phi^{des} P_{sat}(T_{cl})}{p_{a,.cl}} W_{a.cl} - W_{v.cl} \tag{5.1}$$

The molar mass of dry air and vapor is denoted by M_a and M_v, respectively. The humidifier static model computation is made simpler by making the assumption that the humidifier is well controlled. Control schematic for humidifier is shown in Figure 5.3. Equations 5.2 and 5.3, respectively, provide the definitions for the cathode inlet flow rate and pressure calculations.

$$W_{ca,.in} = W_{cl} + W_{v,.inj} = W_{sm.out} + W_{v,.inj} \tag{5.2}$$

$$p_{ca,.in} = p_{a,.cl} + \phi^{des} p_{sat} T_{cl} \tag{5.3}$$

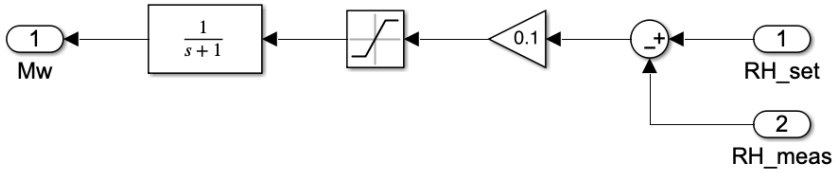

Figure 5.3 : Control diagram for anode humidifer.

5.1.2 Hydrogen supply control

A high-pressure tank supplies the system under study with hydrogen, and a valve controls the rate of discharge. Hydrogen is stored in the fuel reservoir at a pressure of 70 MPa. When the pressure reaches approximately 0.16 MPa, a valve that reduces pressure opens, enabling the release of hydrogen into the fuel cell stack. Excess hydrogen is reintroduced into the stack. The ambient air consists of oxygen (O_2), water vapor (H_2O), and nitrogen (N_2). The cathode network is the term for this. As illustrated in Figure 5.4, a back pressure relief valve allows the exhaust to be released into the atmosphere while maintaining a pressure in the stack of about 0.16 MPa.

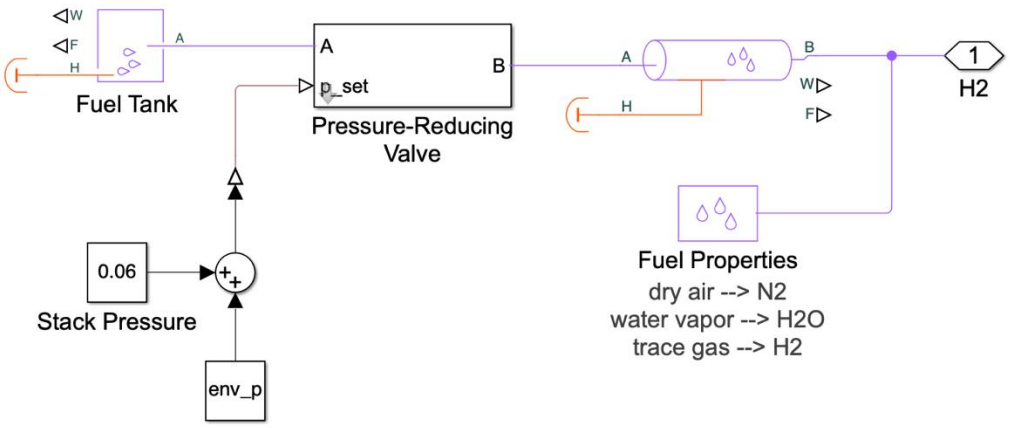

Figure 5.4 : Overview of the Hydrogen Supply

The relative humidity of the incoming hydrogen flux is assumed to be one hundred percent. Reactant pressure and flow rate have a strong correlation in value. In the absence of an additional controller that regulates the flow rate through the graphite channel, a constant pressure induces a fixed gas flow rate into the channel. In order to guarantee that there is an appropriate reactant flow rate to increase system efficiency, a controller is usually utilized to assure the best possible use of the reactants and the power generated during operation. In this work, feedforward current regulation and hydrogen flow rate control are combined since feedforward control systems are faster to respond to changes in the input signal as defined in Figure 5.5. There is an assumed linear relationship between the flow rate and the control signal [60].

$$W_{fcv} = \upsilon_{fcv} W_{fcv.max} \tag{5.4}$$

The control input signal of the valve, denoted as υ_{fcv}, can range from 0 to 1, and the maximum mass flow rate is represented by $W_{fcv.max}$.

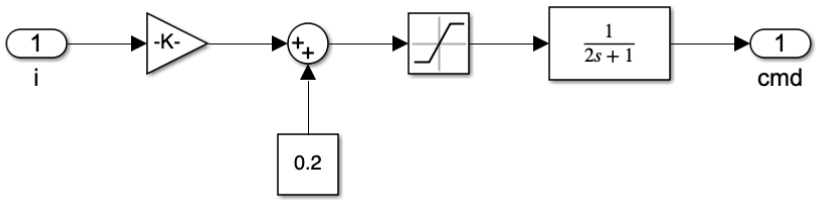

Figure 5.5 : Control diagram for anode recirculation.

Moreover, a purge valve serves as a supplementary control actuator and is commonly located at the terminal end of the anode. Eliminating any built-up liquid water in the

anode is the primary goal of the purge valve, which helps to avoid flooding. The purge valve, as depicted in Figure 5.6, periodically removes the liquid water that builds up in the return manifold. The species flow rates for vapor and hydrogen are as follows:

$$W_{H2,purge} = W_{purge} y_{h2,rm} \tag{5.5}$$

$$W_{v,purge} = W_{purge}(1 - y_{h2,rm}) \tag{5.6}$$

When the water activity in the manifold is greater than one, liquid water will flow via the purge valve from the return manifold. One may calculate the total mass flow rate of water and get the water in liquid form by:

$$W_{l,purge} = (a_{w,rm} - 1) W_{v,purge} \tag{5.7}$$

$$W_{w,purge} = W_{v,purge} + W_{l,purge} \tag{5.8}$$

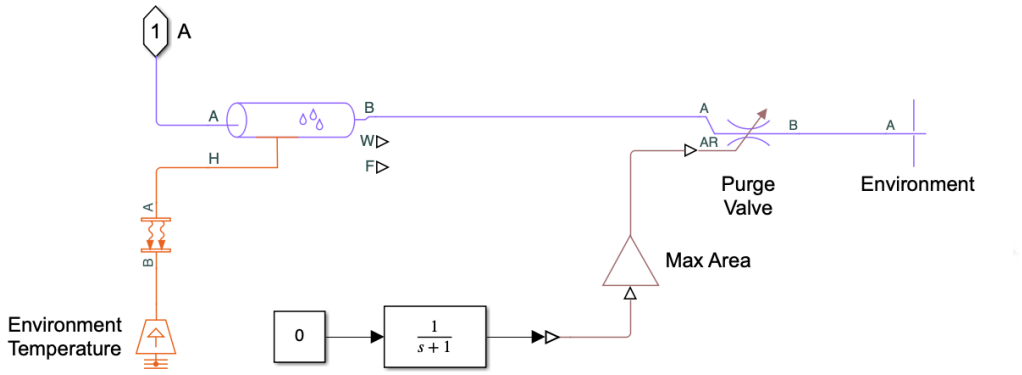

Figure 5.6 : Overview of the anode exhaust.

5.1.3 Oxygen supply control

The air supply system's only control mechanism is a command to the compressor motor. Two factors are used to assess the fuel cell system's control performance: the oxygen concentration in the cathode and the net power of the system. The oxygen excess ratio (OER), λ_{O2}, is defined as the ratio of oxygen supplied to oxygen utilized in the cathode, as given by equation 5.9. It is frequently employed to indicate the excess quantity of airflow that is directed towards the stack.

$$\lambda_{O2} = \frac{W_{O2,in}}{W_{O2,react}} \tag{5.9}$$

Increased oxygen partial pressure, which results from an increased oxygen excess ratio, improves P_{net}. Nevertheless, once an ideal λ_{O2}value is attained, additional elevation will result in an unwarranted surge in compressor power, ultimately weakening the system power. The OER value in this study is 2.5 [61].

If the OER is below 1, it indicates that the oxygen flow rate in the stack is insufficient for the given current value, resulting in an oxygen deficiency in the fuel cell system. If the OER is greater than 1, indicating that the oxygen flow rate in the stack is significantly higher than the necessary amount for a particular current value, then the fuel cell system is in a state of oxygen saturation. Elevated λ_{O2}indicates increased oxygen delivery to the cathode, enhancing the stack's power output. On the other hand, if λ_{O2} is very high, the fuel cell system will reach a state known as "oxygen saturation," which will result in a decrease in net power Pnet due to the compressor's excessive power demands. Because of this, there is an ideal λ_{O2} number that trades off compressor power consumption and stack power production to optimize P_{net}.

The constants and compressor map data used in this investigation were taken from the Pukrushpan et al. study [51]. Figure 5.7 shows compressor map data.

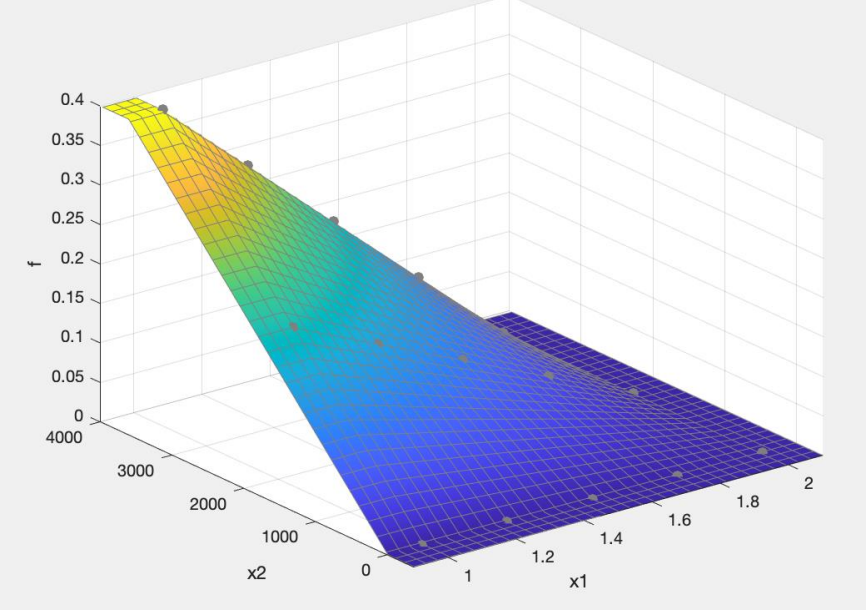

Figure 5.7 : Compressor map data

Since integral control is required to decrease error and proportional control is required to accelerate settling, a PI control is utilized in this paper. Constant oxygen excess ratio control technique is transformed into the output air mass flow rate air $\dot{m_{air}}$ in the outer loop control structure in accordance with the required air mass flow rate $m_{air,des}$

control method. The demanded air mass flow rate, $m_{air,des}$ can come after the wanted air mass, which can be computed using the demanded current Ides. The compressor's real rotating speed in the inner loop control structure is in line with the speed that the PI controller requests. The mechanism allows for quick adjustments to the inner loop's rotational speed. The control procedure that is being used, as shown in Figure 5.8.

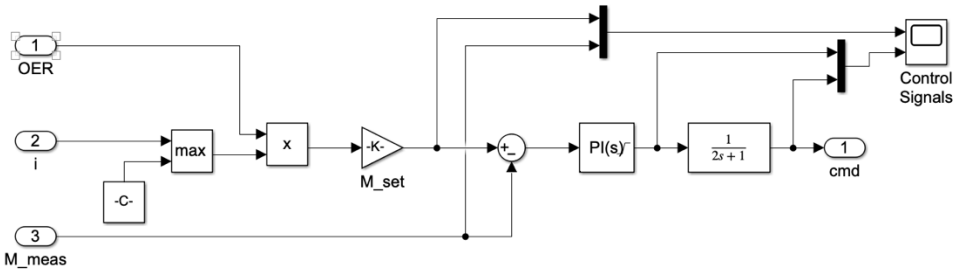

Figure 5.8 : Control diagram for oxygen flow rate through compressor.

The step-response of the PI controller is illustrated in Figure 18. As it can be seen clearly from the graph, over-shooting is observed at 0.008 seconds and reach steady state condition at 0.03 seconds.

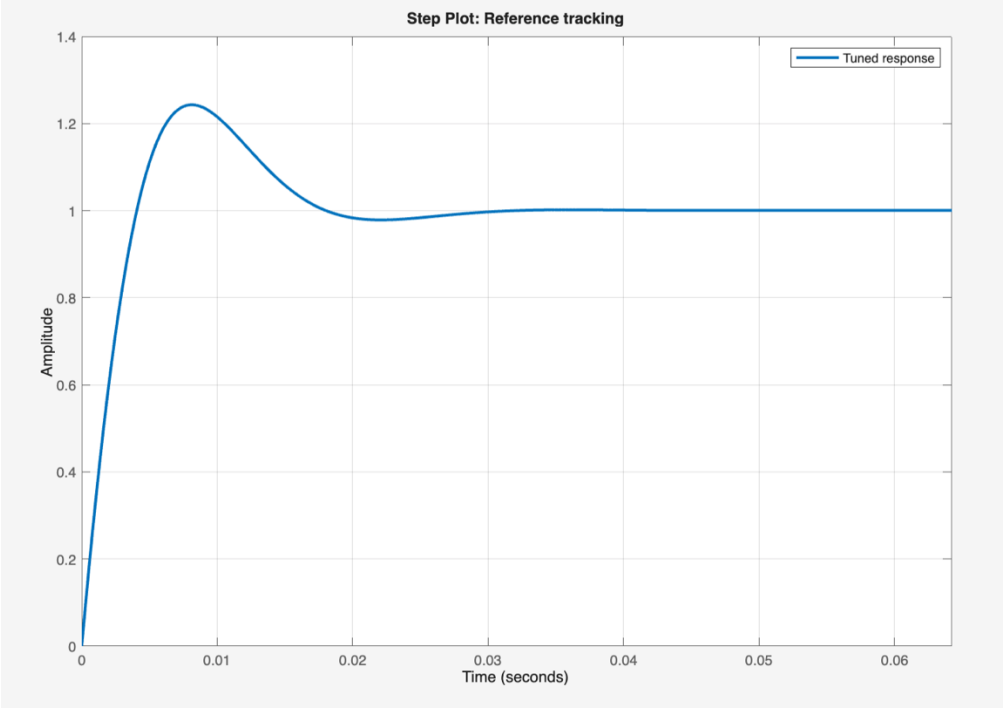

Figure 5.9 : Step response for PI controller.

With regards to mass flow rate of the air controlled by PI controller defined above at downstream of the compressor with respect to time is indicated inFigure 5.9. As it can be interpreted from Figure 5.9 and Figure 5.10, there is a discrepancy between setpoint and measured flow rate until controller reach steady state condition. Following that these data match with each other in a proper manner.

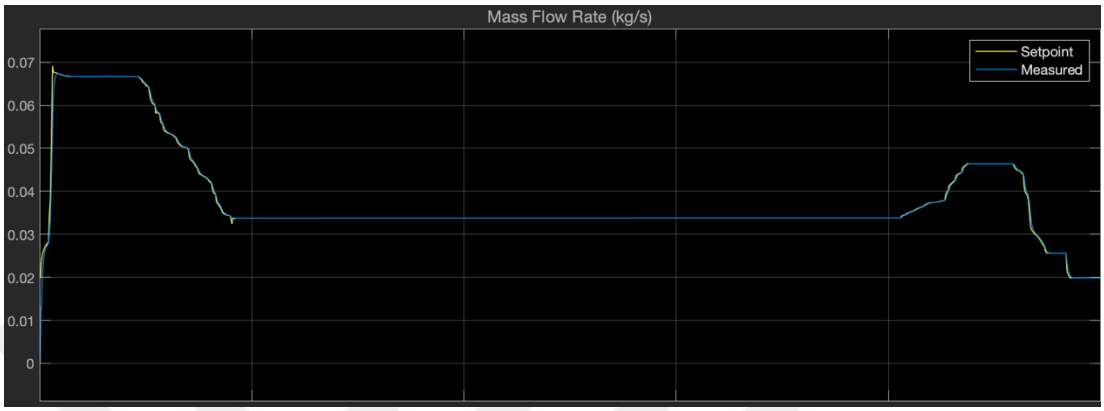

Figure 5.10 : Controlled mass flow rate vs time.

5.1.4 Cooling system control

In order to maintain the system temperature at the desired setpoint, it is necessary to operate a cooling system. A variety of system-integrated cooling devices can be used to achieve cooling. The cooling system under consideration in this work, consisting of a fan and a cooling water pump coupled to a radiator, is used to derive the corresponding model. Figure 3.4 illustrates how the cooling water is routed through the bipolar plate stack's machined water channels and back to the radiator.

Since proportional control is required to accelerate settling and integral control to decrease error, this paper employs the PI control approach to maintain a specified stack temperature of 80 ^{O}C throughout the whole fuel cell process as outlined in Figure 5.11. The step-response of the PI controller being used in pump control is same with controller used on compressor modelling since same parameters are being implemented for control methodology.

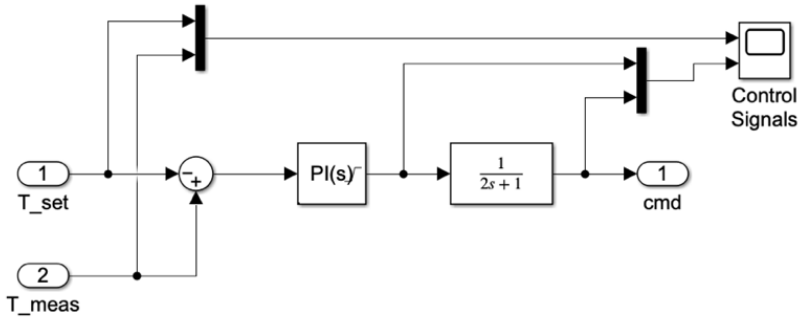

Figure 5.11 : Control of fuel cell temperature.

As it can be interpreted from Figure 5.12, there is a discrepancy between setpoint and measured flow rate until controller reach steady state condition. After that setpoint and measured temperature data are exactly same with each other which means 80^0C target temperature to maintain during whole process is achieved for increasing efficiency of the system.

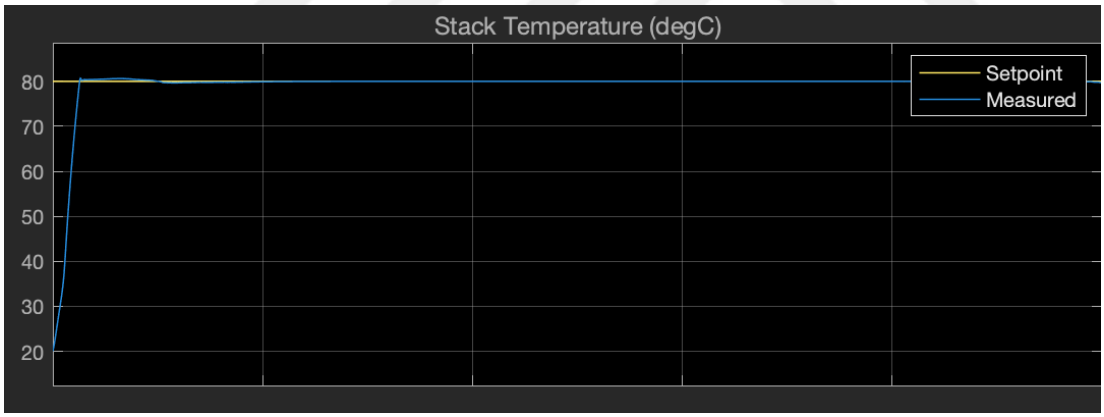

Figure 5.12 : Controlled temperature of the system.

In the light of the auxiliary equipment and stack modelling outlined in Chapter 3 and Chapter 4, the overall fuel stack modelling is generated as illustrated in Figure 5.13.

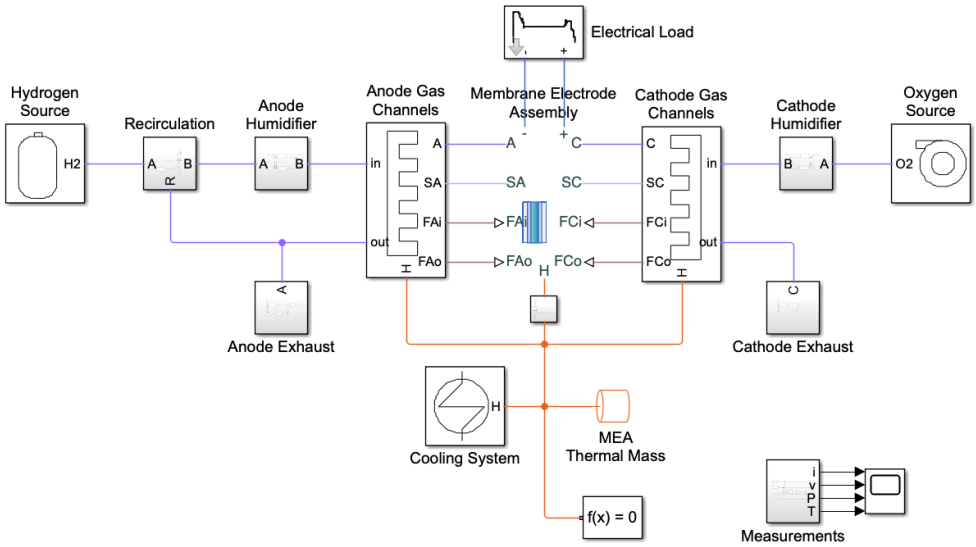

Figure 5.13 PEM fuel cell stack model integrated into the study.

6. RESULTS AND DISCUSSIONS

6.1 Polarization Curve

The Figure 6.1 shows the polarization curve of a fuel cell in the stack. The graph shows that when the current ramps up, electrode activation losses cause an early voltage drop, which is followed by a continuous voltage drop caused by ohmic resistances. The losses incurred during gas transit result in a swift decline in voltage when operating at maximum current. The maximum power output of the fuel cell stack is 76 kW, which can be deduced.

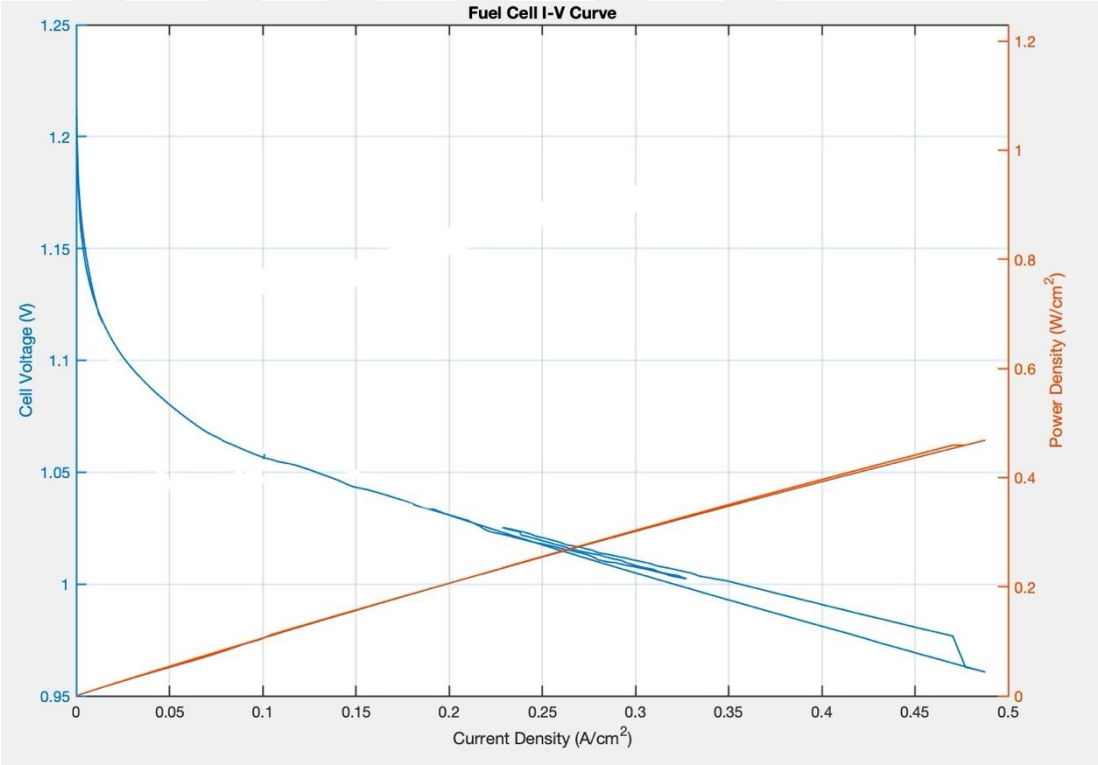

Figure 6.1 Fuel cell I-V curve.

6.2 Power Produced and Heat Dissipated

Furthermore, power generation through electrochemical processes is one of the most important variables to take into account while examining the fuel cell stack model. The electrical power output of the fuel cell stack is graphed together with the power consumption of the coolant pump and cathode air compressor to ensure consistent and

efficient system operation. As a result, the overall power output of the system is slightly lower than the output of the stack. Please note that this model assumes the use of an isentropic compressor. Incorporating the factor of compressor efficiency would lead to a further decrease of two percent in the overall power output. As is evident, the electrical power generated by the fuel cell stack which is shown in Figure 6.2 complies with the demand profile for aircraft as specified in Figure 5.2. The extra heat produced by the fuel cell stack, which the cooling system needs to eliminate, is also depicted in Figure 6.3.

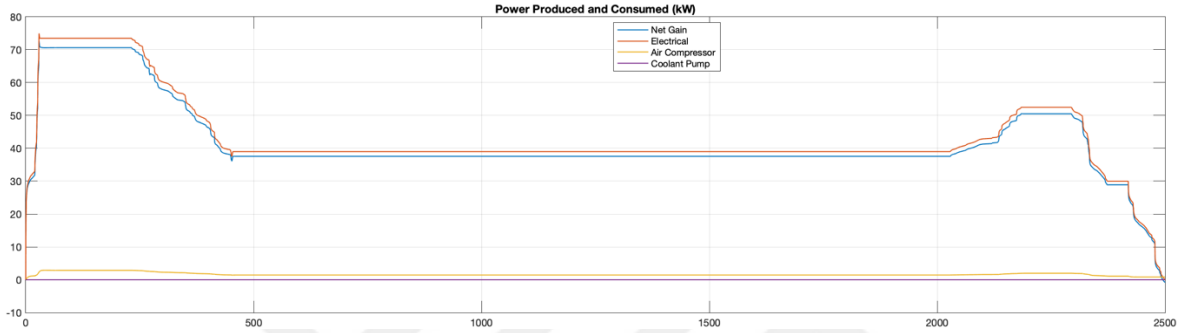

Figure 6.2 Power produced and consumed

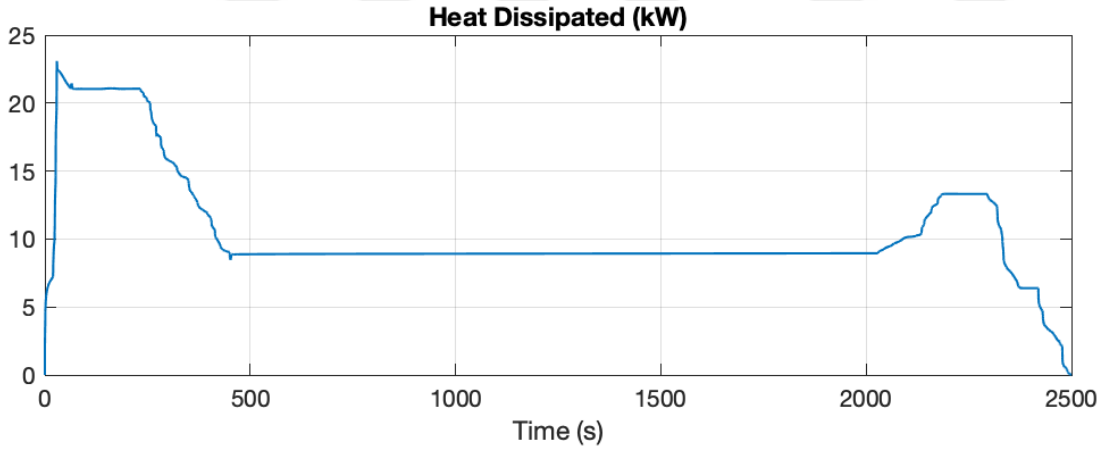

Figure 6.3 Heat dissipation.

6.3 Fuel Cell Efficiency

Fuel cell efficacy is quantified as the proportion of hydrogen consumed to electricity generated. Occasionally, the lower heating value (LHV) of hydrogen (ΔH = 241 kJ/mol) is utilized in place of the higher heating value (HHV) of hydrogen, which is ΔH = 286 kJ/mol. The heat of product water condensation determines the difference between the higher and lower heating values. Both figures are accurate since the

product water can exit the fuel cell as either a liquid or a vapor; the kind of heating value that was utilized to determine the efficiency needs to be mentioned, though [62]. The fuel cell's thermal efficiency is displayed in Figure 6.4. The thermal efficiency quantifies the ratio of hydrogen fuel that has been transformed into productive electrical work by the fuel cell. When running on reformate, well-designed fuel cells can achieve fuel utilization rates of 83% to 85%, and above 90% when running on pure hydrogen [62]. The thermal efficiency (HHV) is approximately 83%.

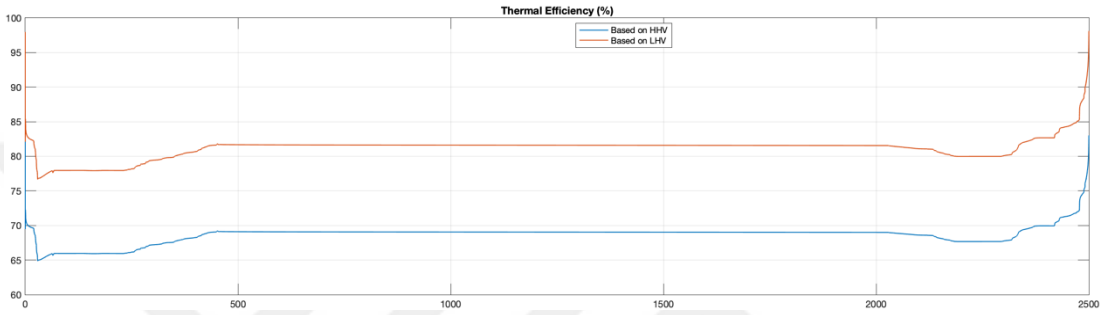

Figure 6.4 Thermal efficiency curve of the system.

6.4 Reactant Utilization

The percentage of reactants (specifically, H_2 and O_2) that are introduced into the fuel cell stack and subsequently converted to fuel through combustion is referred to as reactant utilization. While greater utilization optimizes the consumption of gases in the fuel cell, it concurrently reduces the concentration of reactants and thus diminishes the generated voltage. While any unused oxygen is released into the atmosphere, any unused hydrogen is returned to the anode to avoid wastage. However, in actuality, the H2 is routinely cleansed of impurities. Figure 6.5 illustrates the utilization of both reactants.

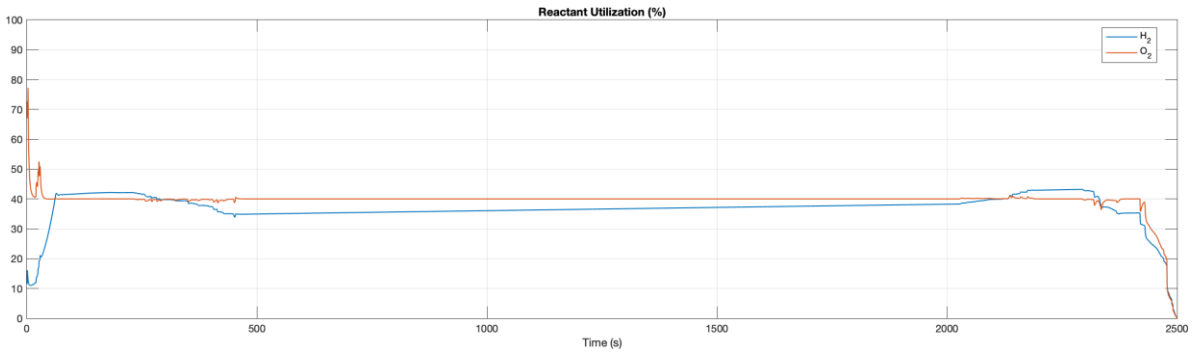

Figure 6.5 Percentile of the reactant utilization.

6.5 Temperature

Figure 6.6 illustrates temperatures at numerous locations throughout the system. The cooling system maintains the temperature of the fuel cell stack at a maximum of 80^0C. The flow that is circulated again heats the fuel that is being directed towards the anode. The compressor raises the temperature of the air that moves towards the cathode. As higher temperatures decrease relative humidity, it leads to an increase in membrane resistance. Therefore, it is crucial to maintain the fuel cell at its optimal temperature. This is important considering the different temperatures experienced by the fuel cell at different locations. In this model, the flow rate of the coolant pump is regulated to operate the cooling system. Figure 6.7 also shows the coolant temperature after it absorbs heat from the fuel cell stack and releases heat in the radiator.

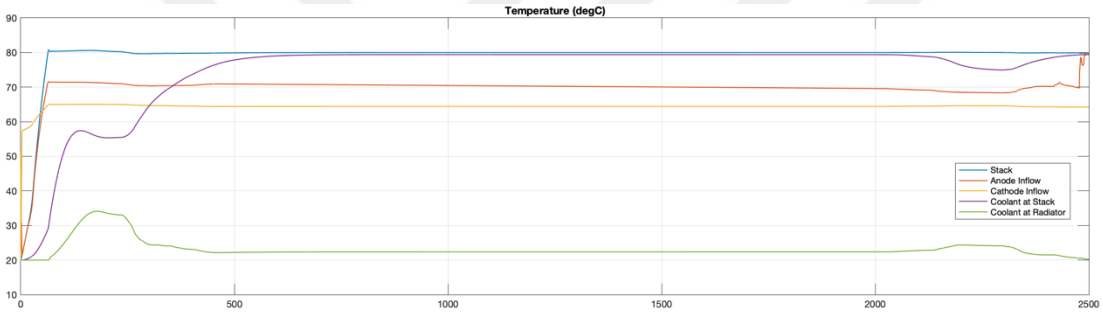

Figure 6.6 Temperature of parts of the PEM fuel cell stack.

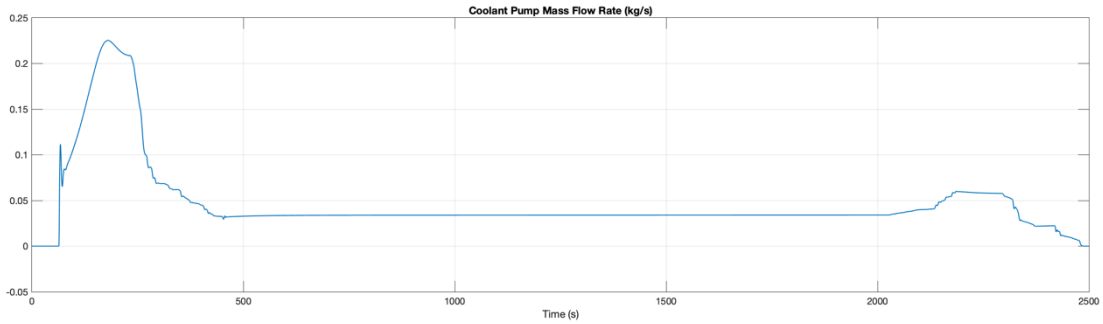

Figure 6.7 Mass flow rate of the coolant pump.

6.6 Hydrogen Consumption

Figure 6.8 displays the hydrogen mass utilized during operation, together with the accompanying reduction in hydrogen tank pressure and the conversion of energy from hydrogen fuel usage to electrical energy.

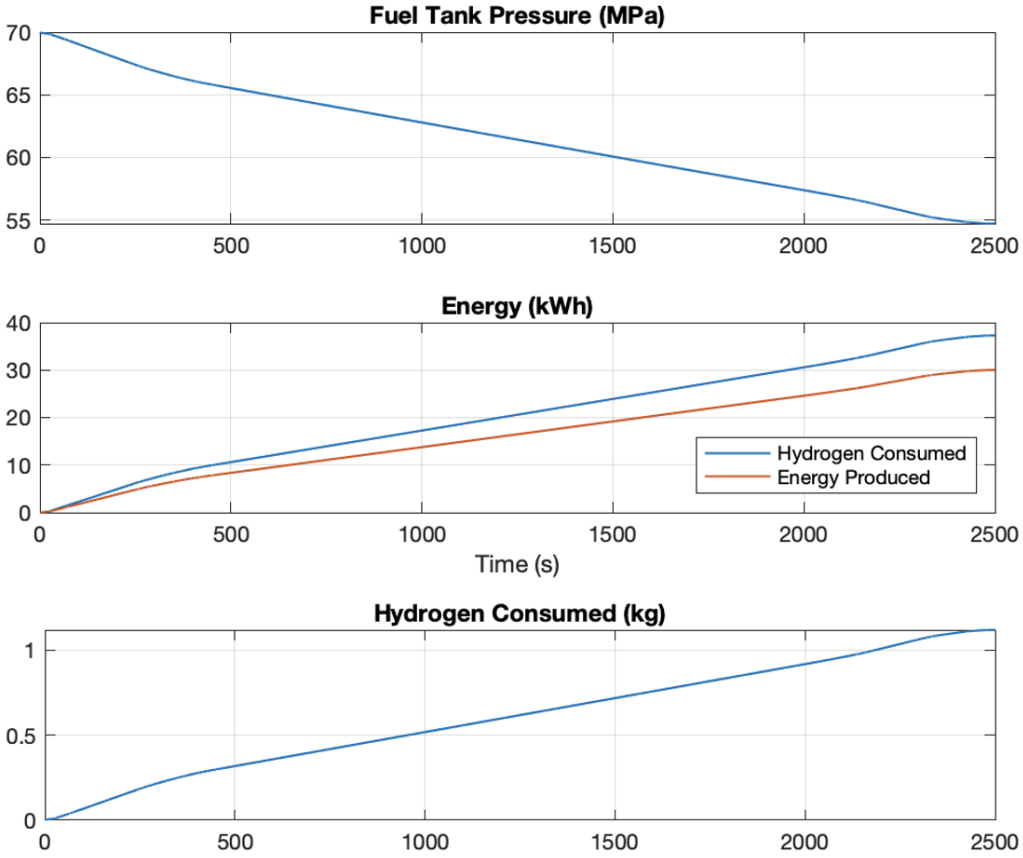

Figure 6.8 Hydrogen consumption&tank pressure&energy converted.

6.7 System Simulation Results

The Figure 6.9 shows the current, voltage, power (electrical and heat) and stack temperature with regards to time.

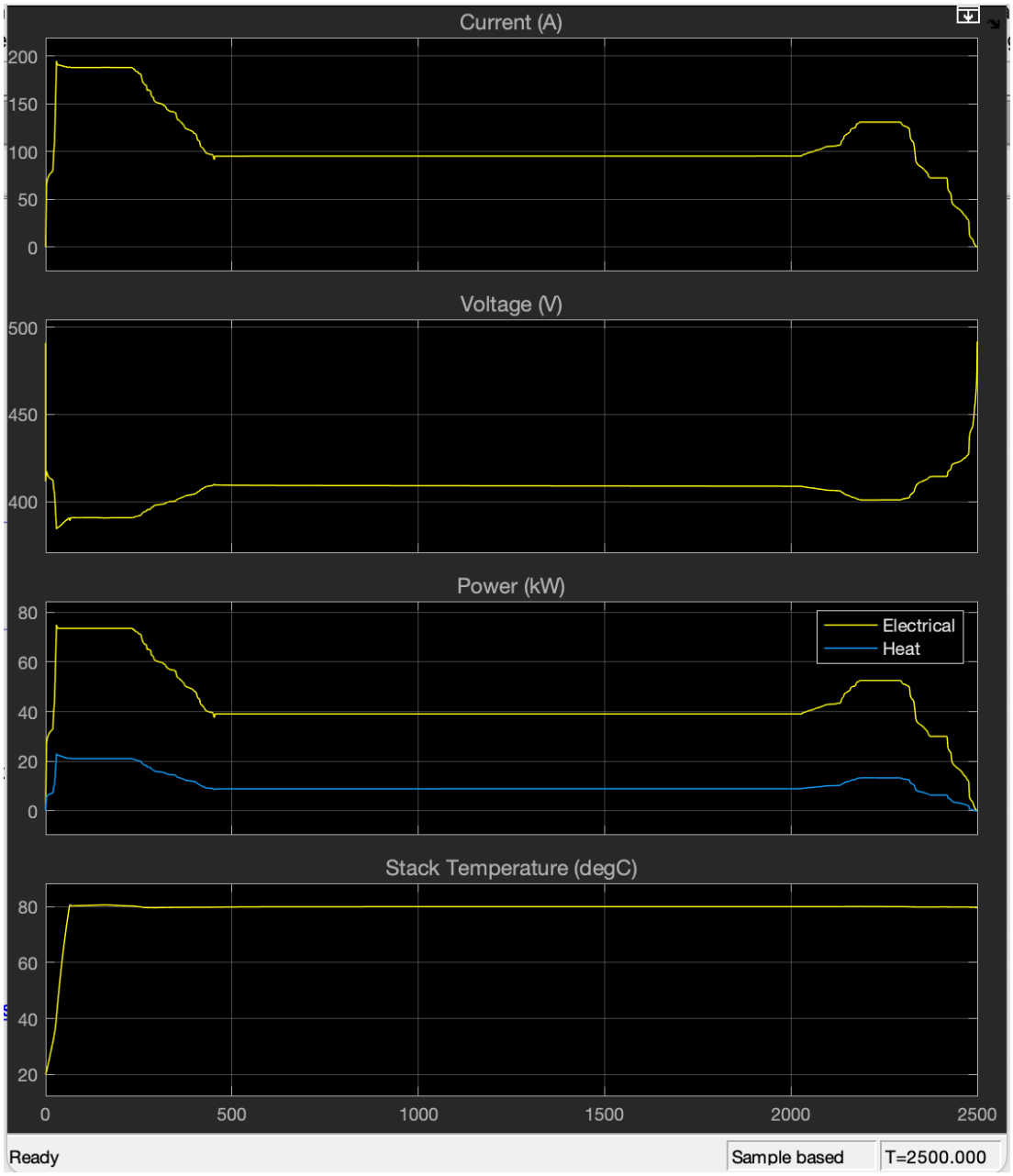

Figure 6.9 Simulink scope.

7. CONCLUSION AND FUTURE WORKS

To meet the electrical power consumption profile defined for the MQ-1 Predator UAV, this thesis conducts control experiments and models PEM fuel cells. Reactant flow rate control on both the anode and cathode sides is the primary control methodology used in this investigation. The fuel cell stack model includes a developed membrane electrode assembly together with ancillary machinery such a cooling system, humidifier, compressor, and recirculation system. The models found in the literature that use the proportionate control mechanism on both the anode and cathode sides were the basis for developing the humidifier model. The compressor model is directly lifted from the literature, with double-loop control implemented and air flow regulated by feedback linked static controller. Additionally, a recirculation model that uses feedforward-based control to utilize exhaust gas that is available downstream of the anode is adapted from the literature. In addition to the auxiliary equipment, the stack voltage model is designed to compute the stack voltage based on the stack current and estimate the losses experienced in the polarization curve. According to this analysis, the compressor and coolant pump work causes the system's net power to be a few percent less than the stack's power. Future research may combine a fuel cell and battery to simulate a hybrid system that would deliver net power equivalent to meeting aircraft demand using a non-isentropic compressor. Furthermore, a purge valve with control logic might be used to maintain a high hydrogen concentration on the anode side. Purge valve integration and exhaust hydrogen control will be beneficial for overall system performance because higher nitrogen concentrations are correlated with lower hydrogen concentrations and lower fuel cell efficiency.

REFERENCES

[1] Air | Mobility and Transport. [Online]. Available: <https://ec.europa.eu/transport/modes/air_en. [Accessed 26 January 2019].

[2] Current market outlook. 2017-2036 [Online]; Available: <http://www.boeing.com/resources/boeingdotcom/commercial/market/current-market-outlook-2017/assets/downloads/2017-cmo-6-19.pdf. [Accessed 05 May 2018].

[3] **Gizem Sürer M, Arat H Turan.** State of art of hydrogen usage as a fuel on aviation. Eur Mech Sci 2018;2(1):20–30.

[4] **Bicer Y, Dincer I.** Life cycle evaluation of hydrogen and other potential fuels for aircrafts. Int J Hydrog Energy 2017;42(16):10722–38.

[5] Facts and figures, air transport action group, May. [Online]; 2018. Available: <https://www.atag.org/facts-figures.html. [Accessed 05-May-2018].

[6] **Koroneos C, Dompros A, Roumbas G, Moussiopoulos N**. Life cycle assessment of kerosene used in aviation (8 pp). Int J Life Cycle Assess 2005;10(6):417–24.

[7] **Wilberforce T, Alaswad A, Palumbo A, Dassisti M.** Advances in stationary and portable fuel cell applications. Int J Hydrog Energy 2016;41(37):16509–22.

[8] **Baroutaji A, Carton J, Stokes J, Olabi A-G.** Design and development of proton ex- change membrane fuel cell using open pore cellular foam as flow plate material. Energy Chall Mech North Sea Conf J LTD 2014.

[9] **Baharozu E, Soykan G**. Future aircraft concept in terms of energy efficiency and environmental factors. Energy 2017;140:1368–77.

[10] **Dincer I, Acar C.** A review on potential use of hydrogen in aviation applications. Int Sustain Aviat 2016;2(1):74.

[11] **Thirkell, Alex. 2021.** "Systems Study for Fuel Cell Powered More Electric Aircraft". Loughborough University. https://doi.org/10.26174/thesis.lboro.14758005.v1.

[12] **K.A.I.L.Wijewardena Gamalath, B.M.P. Peiris.** Theoretical Approach to the Physics of Fuel Cells. International Letters of Chemistry, Physics and Astronomy.2012;15-22.

[13] **C. Bonnet, S. Didierjean, N. Guillet, S. Besse, T. Colinart, P. Carre.** Design of an 80kWe PEM fuel cell system: Scale up effect investigation. Journal of Power Sources.182 (2008); 441–448.

[14] **D. Verstraete, K. Lehmkuehler, A. Gong, et al.,** Characterisation of a hybrid, fuel-cell-based propulsion system for small unmanned aircraft. Journal of Power Sources, 2014. 250: p. 204-211.

[15] **Jay T. Pukrushpan, Anna G. Stefanopoulou, and Huei Peng.** Modeling and Control for PEM Fuel Cell Stack System. in Proceedings of American Control Conference. 2002. 4, 3117-3122.

[16] **R.E. Rosli**, **A.B. Sulong**, **W.R.W. Daud**, **M.A. Zulkifley**, **M.I. Rosli**, **E.H. Majlan**, **M.A. Haque**. Reactant Control System for Proton Exchange Membrane Fuel Cell. 4th International Conference on Process Engineering and Advanced Materials. 2016: 615 – 620.

[17] **Thirkell, Alex**."Systems Study for Fuel Cell Powered More Electric Aircraft". Loughborough University. 2021. https://doi.org/10.26174/thesis.lboro.14758005.v1.

[18] **S.Yasemin.** Modeling And Control Of A Pem Fuel Cell System. Master Thesis on The Graduate School of Natural And Applied Sciences Of Middle East Technical University.2013.

[19] **Nieves Lapena-Rey, Jonay Mosquera, Elena Bataller, et al**. Environmentally friendly power sources for aerospace applications. Journal of power sources, 2008. 181(2): p. 353-362.

[20] **Hemighaus, G., Boval, T., Bosley, C., Organ, R., Lind, J. B., Thompson, T., et al. (**2006). Alternative Jet Fuels. Chevron Corporation.

[21] **Klug, H. G.** (2000). Cryoplane-Hydrogen Fuelled Aircraft. Hamburg: EADS Airbus GmbH.

[22] **Westenberger, A.** (2007a). H2 Technology for Commercial Aircraft. Hamburg: Airbus Deutschland GmbH.

[23] **EC.** (2012, 02 20). H2 Aircraft - Cryoplane and future of flight. Retrieved 04 16, 2013, from European Commission - Research & Innovation: http://ec.europa.eu/research/transport/projects/items/h2aircraft___cryo plane_and_the_future_of_flight_en.htm

[24] **Belmonte N, Staulo S, Fiorot S, Luetto C, Rizzi P, Baricco M.** Fuel cell powered octocopter for inspection of mobile cranes: design, cost analysis and environmental impacts. Appl Energy 2018;215:556–65.

[25] Fuel cell and hybrid power systems offer compelling value for UAVs whose missions demand greater runtime than batteries can support. [Online]. Available: http:// www.ballard.com/markets/uav. [Accessed 05 May 2018].

[26] AeroVironment flies world's first hydrogen powered plane. Fuel Cells Bull. vol, no. 9; 2005. p. 2–3.

[27] **Bradley TH, Moffitt BA, Mavris DN, Parekh DE.** Development and experimental characterization of a fuel cell powered aircraft. J Power Sources 2007;171(2):793–801.

[28] **Gong A, Verstraete D.** Fuel cell propulsion in small fixed-wing unmanned aerial vehicles: current status and research needs. Int J Hydrog Energy 2017;42(33):21311–33.

[29] **Kim T, Kwon S.** Design and development of a fuel cell-powered small unmanned aircraft. Int J Hydrog Energy 2012;37(1):615–22.

[30] Boeing fuel cell plane in manned aviation first. Fuel Cells Bull. vol, no. 4; 2008. p. 1.

[31] First flight of DLR's HY4 fuel cell light aircraft. Fuel Cells Bull. vol, no. 10; 2016. p. 1.

[32] **L.L. Kohout, P.C. Schmitz**. An Analysis of Fuel Cell Options for an All-Electric Unmanned Aerial Vehicle, NASA/TM—207-214699, 2007.

[33] **Anubhav Datta.** PEM Fuel Cell Model for Conceptual Design of Hydrogen eVTOL Aircraft. NASA/CR—20210000284

[34] **S. Thomas, M. Zalbowitz.** Fuel Cells Green Power, Los Alamos National Laboratory, 2006.

[35] **Bicer Y, Dincer I**. Life cycle evaluation of hydrogen and other potential fuels for aircrafts. Int J Hydrog Energy 2017;42(16):10722–38.

[36] **L.F. Brown**. Comparative study of fuels for on-board hydrogen production for fuel-cell-powered automobiles. *International Journal of Hydrogen Energy*, 26, 381-397, 2001

[37] J**. Zhang, Z. Xie, J. Zhang, Y. Tang, C. Song, T. Navessin, Z. Shi, D. Song, H. Wang, D. Wilkinson, Z. Liu, S. Holdcroft**. High temperature PEM fuel cells. *Journal of Power Sources*, 160, 872-891, 2006

[38] **J. Larminie, A. Dicks, Wiley.** Fuel Cell Systems Explained, Second Edition, Publication, 2003

[39] Editorial Polymer electrolytes for a hydrogen economy., Internal Journal of Hydrogen Energy 2012, 37, 6120-613.

[40] **Smitha B., Sridhar A., Khan A.A**., Solid polymer electrolyte membranes for fuel cell applications-a review., Journal of Membrane Science 2005, 259, 10-26.

[41] **Fernandes A.C., Ticianelli E.A.,** A performance and degradation study of Nafion 212 membrane for proton exchange membrane fuel cells., Journal of Power Sciences 2009,193, 547-554.

[42] **Othman R., Dicks A.L., Zhu Z.,** Non precious metal catalysts for the PEM fuel cell cathode., International Journal of Hydrogen Energy 2012,37, 357-372.

[43] **Litster S., McLean G.,** PEM fuel cell electrodes., Journal of Power Sources 2004, 130, 61–76.

[44] **Bayrakçeken A., Erkan S., Türker L., Eroğlu İ**., Effects of membrane electrode assembly components on proton exchange membrane fuel cell performance, International Journal of Hydrogen Energy 2008,33, 165 – 170.

[45] **Barbir F.,** PEM Fuel Cells: Theory and Practice. Elsevier Inc., 2005.

[46] **Park S., Lee J., Popov B.N**., A review of gas diffusion layer in PEM fuel cells: Materials and designs., International Journal of Hydrogen Energy 2012,37,5850-5865.

[47] **Antunes R.A., Oliveira M.C.L.,** Ett G., Ett V., Corrosion of metal bipolar plates for PEM fuel cells: A review., International Journal of Hydrogen Energy 2010,35, 3632-3647.

[48] **Yang X., Ye Q., Cheng P.,** Hydrogen pumping effect induced by fuel starvation in a single cell of a PEM fuel cell stack at galvanostatic operation., International Journal of Hydrogen Energy 2012,37, 14430-14453.

[49] **Yousfi-Steiner N., Moçotéguy P., CandussoD., Hissel D.,** A review on polymer electrolyte membrane fuel cell catalyst degradation and starvation issues: Causes, consequences and diagnostic for mitigation., Journal of Power Sources 2009, 194, 130–145.

[50] **Matraji I., Laghrouche S., Jemei S., Wack M**., Robust control of the PEM fuel cell air-feed system via sub-optimal second order sliding mode., Applied Energy 2013,104, 945-957.

[51] **Pukrushpan J.T., Stefanopoulou A.G**., Peng H.,Control of Fuel Cell Power Systems. Principles, Modeling, Analysis and Feedback Design,Springer.2004.

[52] **Vega-Leal A.P., Palomo F.R., Barragán F., García C., Brey J.J**., Design of control systems for portable PEM fuel cells., Journal of Power Sources 2007,169, 194-197.

[53] **Park Y. H., Caton J. A..,** Development of a PEM stack and performance analysis including the effects of water content in the membrane and cooling method., Journal of Power Sources2008, 179, 584-591.

[54] **Incropera, DeWitt., Bergman., Lavine.,** Fundamentals of Heat and Mass Transfer..6th edition.Wiley 2007.

[55] **Adams, J., Yang, W.-C., Oglesby, K., and Osborne, K**. (2000). The development of Ford's P2000 fuel cell vehicle. SAE Paper 2000-01-1061.

[56] **Zhu Y, Cai W, Wen C, Li Y**. Fuel ejector design and simulation model for anodic recirculation SOFC system. J Power Sources 2007;173:437–49.

[57] **J. C. Amphlett, M. Baumertr, and F. Mannr,** "Performance modeling of the Ballard mark IV solid polymer electrolyte fuel cell: Empirical model development," J. Electrochem. Soc., vol. 142, no. 1, pp. 9–15, Jan. 1995.

[58] **J. Kim, M. Lees, and S. Srinivasan,** "Modeling of proton exchange membrane fuel cell performance with an empirical equation,"

[59] **Thirkell, Alex. 2021**. "Systems Study for Fuel Cell Powered More Electric Aircraft". Loughborough University. https://doi.org/10.26174/thesis.lboro.14758005.v1.

[60] **He J., Ahn J., Choe S.,** Analysis and control of a fuel delivery system considering a two-phase anode model of the polymer electrolyte membrane fuel cell stack., Journal of Power Sources 2011, 196, Issue 10, 4655-4670.

[61] **Frano Barbir.** Vehicles With Hydrogen Air Fuel Cells, Vol II, Encyclopedia of Life Support Systems (EOLSS).

[62] **Frano Barbir.** PEM Fuel Cells, Chapter 3 Fuel Cell Chemistry, 2005:33-72.

CURRICULUM VITAE

Name Surname **: OSMAN SÖZEN**

EDUCATION **:**

- **B.Sc.** **:** 2018, Yıldız Technical University, Faculty of Engineering , Department of Mechanical Engineering

Undergraduate Thesis:

- Design of Air Conditioning Plant and Selection of Equipment for a Social Facility in İzmir